NOMA for Multi-Cell RIS Networks: A Stochastic Geometry Model

Chao Zhang, *Member, IEEE,* Wenqiang Yi, *Member, IEEE,* Yuanwei Liu, *Fellow, IEEE,*
Zheng Ma, *Member, IEEE* and Xingqi Zhang, *Member, IEEE*

***Abstract*—This paper investigates reconfigurable intelligent surface (RIS) aided multi-cell non-orthogonal multiple access (NOMA) networks with stochastic geometry methods. Under Rayleigh and Nakagami-m fading channels, we provide two types of approximate channel models to depict RIS channels, i.e., the N-fold convolution model and the curve fitting model. The analysis reveals that the N-fold convolution model is accurate and tractable when ignoring inter-cell interference, while the curve fitting model can evaluate the impact of inter-cell interference with a small error. The N-fold convolution model provides accurate diversity orders compared to other existing approaches such as the central limit model. Based on these channel models, we derive the closed-form analytical and asymptotic expressions of coverage probabilities and ergodic rates for two paired NOMA users. The analytical results demonstrate that: i) When we ignore inter-cell interference, the diversity order of the typical user is equal to the number of Rayleigh fading channels; and ii) For Nakagami-m fading channels with coefficient m, the diversity order is equal to m times of the channel number. Numerical results show that: i) RISs are capable of enhancing the coverage performance and ergodic rates of the proposed network; and ii) RISs provide extra flexibility for NOMA decoding orders.**

***Index Terms*—Multi-cell NOMA, reconfigurable intelligent surface, stochastic geometry**

I. Introduction

Compared to the fifth-generation (5G) mobile communication to fulfill emergencies such as massive throughput and low latency transmission [2], [3], a controllable wireless communication environment is important for the sixth-generation (6G) of mobile communication networks [4]. To achieve the "smart radio environments" [5], reconfigurable intelligent surface (RIS) is a promising technology by reconfiguring radiation signals, which has rekindled the interest of researchers due to the ability of integration.

Non-orthogonal multiple access (NOMA) introduces enhanced connectivity to communication systems through dynamic power allocation and successive interference cancellation (SIC) techniques. Despite its impressive potential for achieving substantial throughput, the NOMA technique encounters various implementation challenges, as highlighted in previous research [6]. Particularly, the introduction of NOMA brings about supplementary interference, resulting in compromised quality of service (QoS) for users situated at the cell edges in contrast to those in orthogonal multiple access (OMA) networks. Furthermore, the rigidity of SIC orders for selected NOMA users poses limitations due to its dependence on individual channel qualities. This inflexibility can lead to unfavorable scenarios, such as pairing a weak user with high QoS demands alongside a stronger user. In such cases, the performance of the weaker NOMA user tends to be inferior compared to an OMA scenario.

To overcome these shortcomings, RISs offer a viable solution. By leveraging RISs to enhance channel quality, the performance of cell-edged users experiences a notable uplift. Additionally, the incorporation of RISs introduces a malleable aspect to the ranking of channel quality. This adaptability becomes especially evident when segments of NOMA users benefit from RIS assistance. Consequently, the flexibility in SIC orders mitigates the interference challenges posed by the SIC process. In light of these advancements, RIS-aided NOMA networks emerge as a promising avenue for the future of 6G programmable communication and multiple access paradigms.

To achieve "smart radio environments" with massive connectivity, one of the priorities is to derive tractable and accurate channel distributions for RIS-aided channel models. An RIS achieves phase shifting by controlling the phase of incident electromagnetic waves on its reflecting elements. Channel estimation is critical for optimizing the RIS's behavior, involving the use of known pilot signals to estimate the channel response between the transmitter, RIS, and receiver. The RIS then adjusts its phase shifts based on the estimated channel information to enhance communication performance.

One controversy is whether the RISs are regarded as whole linear materials or antenna elements [7], [8]. Furthermore, the models that describe large-scale fading, commonly known as path loss models, can be broadly categorized into two main types: near-field models and far-field models. For the scope of this paper, our emphasis is placed on the far-field scenario, allowing us to allocate more dedicated attention to comprehensively analyzing the performance within the near-field context. Moreover, although several channel models are proposed in recent works, tractable channel models for multi-cell networks are still in their infancy as the complexity is significantly enhanced. Hence, the main challenge is *"how to find a tractable and accurate channel model for RIS-aided*

C. Zhang and Y. Liu are with the School of Electronic Engineering and Computer Science, Queen Mary University of London, London, E1 4NS, United Kingdom. (email: {chao.zhang, yuanwei.liu}@qmul.ac.uk).

W. Yi is with the School of Computer Science and Electronic Engineering, University of Essex, Colchester, CO4 3SQ, United Kingdom. (email: w.yi@essex.ac.uk).

Z. Ma is with the Provincial Key Laboratory of Information Coding and Transmission, Southwest Jiaotong University, Chengdu, 611756, Sichuan, China. (e-mail: zma@swjtu.edu.cn).

X. Zhang is with the Department of Electrical and Computer Engineering, University of Alberta, Edmonton AB, T6G 2R3, Canada. (e-mail: xingqi.zhang@ualberta.ca).

Part of this work was accepted in IEEE International Conference on Communications (ICC), Montreal, Canada, June, 2021 [1].

multi-cell NOMA networks".

A. Related Works

This section provides the related works for RISs and NOMA networks.

1) Related Works for RISs: Recent research contributions have evaluated the RIS-aided networks in several aspects. For information-theoretic fundamentals of RIS-aided networks, different channel models including propagation and path loss modeling have been proposed [7]–[10]. Additionally, various specific path loss models are provided by [8]. More specifically, the channel models for linear materials have been proposed and investigated by [7], [10], and other papers focused on RIS models with antenna elements [8], [9]. Based on the existing channel models in current works, contributions to different applications are summarized in the following. One breakthrough for RISs is the passive beamforming design [11]–[15], which is the main focus of RIS-aided systems. Several aspects of technologies have provided theoretical basics for performance analysis, including passive beamforming [15], information transfer [13], modulation [16], and resource allocation [14]. Additionally, research papers of RIS applications in different scenarios have indicated the benefit that RISs have high compatibility, such as RISs combined with machine learning methods [17], [18], RIS-aided mmWave networks [19], [20], and RIS-aided internet of things (IoT) networks [21].

2) Related Works for RIS-aided NOMA: Since RISs enhance the performance of NOMA networks and provide the flexibility of SIC orders, recent RIS-aided NOMA networks have received heated discussions in the research community [22]. In physical layer analysis for RIS-aided NOMA networks, valuable contributions have been provided with various approaches, directions, and scenarios. Firstly, beamforming designs for RIS-aided NOMA networks have been investigated to meet the characteristics of NOMA in [23]. Based on the beamforming designs, the outage performance of a single-cell RIS-NOMA network has been evaluated in [24]. With the aid of the aforementioned efforts, different channel models have been derived: i) by the "central limit theorem to calculate the approximated expressions and limits [25]; and ii) by the 'N-fold convolution' to obtain the asymptotic expressions with diversity orders [26] for single-cell scenarios.

We draw a clear distinction between our study and the work presented in [10], [27]. The paper [10] also explores multi-cell aided NOMA networks while their approach entails modeling RISs as linear materials. This stands in contrast to our paper's consideration of RISs containing numerous individual elements, a more comprehensive approach in our current investigation. Moreover, the authors of [27] have evaluated the performance of RIS-assisted multi-cell networks using stochastic geometry models, presenting insights into the application of stochastic geometry models in RIS-aided networks. With different motivations, our study centers on NOMA networks and seeks to leverage RISs to enhance the performance of weaker users, given that cell-edge user performance is typically inferior in NOMA networks compared to OMA cases. With this motivation, our paper delves into investigating RIS-aided multi-cell NOMA networks, with a unique focus on viewing RISs as individual elements rather than an entire linear material.

B. Motivation and Contribution

We aim to exploit RISs to provide additional flexibility of SIC orders in NOMA networks and to combine the techniques to achieve massive connectivity. Considering RISs are made of sub-wavelength-sized elements, we investigate RIS-aided NOMA networks in multi-cell scenarios to evaluate the coverage performance and ergodic rates. In this paper, we consider the 'product of distances' model to present the path loss model. We additionally invoke stochastic geometry methods to analyze the spatial effects of users and base stations (BSs). Hence, the main contributions are summarized as follows:

- We derive two types of channel models of RIS links (including reflection links and direct links). For the first type of channel model, we utilize "N-fold convolution" to derive asymptotic expressions, followed by diversity orders when ignoring inter-cell interference. With the aid of the curve fitting tools, we derive a channel model exploited in multi-cell scenarios. We additionally extend the models from Rayleigh fading channels to Nakagamim fading channels. By modeling the multi-cell networks as two homogeneous Poisson point processes (HPPPs), we investigate the spatial effects of networks.
- We then derive the closed-form analytical expressions for the coverage probabilities of the typical user and the connected user, respectively. To investigate the impact of RISs, we analyze the asymptotic performance for the typical users versus the number of RIS elements n and transmit power P_t. The analytical results reveal that increasing the number of RIS elements is able to enhance the coverage probability.
- We additionally derive the closed-form analytical expressions for ergodic rates of NOMA users. Moreover, the asymptotic analysis is provided, which reveals that the achievable rates reach upper limits with a large number of RIS elements or a large transmit power level.
- We verify our analytical results by Monte Carlo simulations. Numerical results demonstrate that: i) RISs enhance the coverage performance and ergodic rates of NOMA networks; ii) The SIC orders of NOMA networks enable to be altered with the aid of RISs; and iii) For multi-cell scenarios, the NOMA users have upper limits of the performance (including coverage performance and ergodic rates) because of the interference from other cells.

C. Organizations

This paper is organized into the following sections. In Section II, we introduce the signal model with stochastic geometry methods. In Section III, we derive the channel models, including an asymptotic analytical model to derive the diversity orders and a curve fitting model to fit multi-cell scenarios. In Section IV, we derive the analytical coverage probability as closed-form expressions for a typical user and a connected user in a NOMA pair. We additionally derive

the asymptotic coverage probability expressions of the typical user to investigate the effect of RISs. In Section V, ergodic rate performance is investigated by deriving closed-form analytical and asymptotic expressions. We present numerical results in Section VI, followed by Section VII as a conclusion.

II. System Model

This paper uses stochastic geometry models to study how space affects long-term average performance. When a user has already connected to a BS, other users are randomly joining in this channel with the aid of NOMA. As for the practical implementation, the first coming user will be paired with the connected user. We investigate a RIS-aided multi-cell NOMA network, which includes randomly distributed BSs, users, and fixed RISs. We evaluate a two-user NOMA pair in this treatise, where different NOMA pairs are served by orthogonal resource blocks to cancel inter-cell interference[1]. In practical scenarios, this paper focuses on a connected user continuously connecting within a BS, while other users join using NOMA. This involves a fixed connected user and dynamically joining typical users forming NOMA pairs. The typical users are randomly chosen from a point process. The RIS remains stationary on structures like tall buildings. This establishes a premise where typical users and BSs follow HPPP distributions, while connected users and RISs remain fixed at known distances.

A. Deployment of Devices

Applying stochastic geometry, we employ two independent HPPPs to model users and BSs: i) $\Phi_u \subset \mathbb{R}^2$ with a density of λ_u representing users; and ii) $\Phi_b \subset \mathbb{R}^2$ with density λ_b depicting BSs. The typical user serves as the reference point at origin O on the plane. For simplicity, we assume a fixed distance r_{RU} between the user and its nearby RIS, while the distance from the connected BS to the RIS is defined as r_{BR}. A connected user, located at $\mathbf{x}_C$, is already associated with the BS. Consequently, this user is excluded from the Φ_u set, and its distance to the BS remains constant at r_c.

We assume $r_{RU} \ll r_{BR}$ since the RIS is allocated near to the typical user. Hence, the distances r_{BR} and r_{BU} are approximately equal, i.e., $r_{BR} \approx r_{BU}$. The association criterion for the typical user is to select the BS with the strongest received power. This means that the distance between the RIS and the associated BS is the nearest under the above assumptions, i.e., $\mathbf{x}_{B,near} = \arg\min \mathbf{x}_B \in \Phi_b \, |\mathbf{x}_B|$, where $|\cdot|$ is the magnitude or absolute value. Based on the definition that the position of the typical user is regarded as the origin, the communication distances from the typical user to the RIS (at $\mathbf{x}R$) and the associated BS (at $\mathbf{x}_{B,near}$) are denoted as $r_{RU} = |\mathbf{x}_R|$ and $r_{BU} = |\mathbf{x}_{B,near}|$, respectively. Therefore, the distance between the associated BS and the RIS is given by $r_{BR} = |\mathbf{x}_{BR}| = |\mathbf{x}_{B,near} - \mathbf{x}_R|$, where $\mathbf{x}_{BR}$ is the distance vector between the BS and the RIS.

[1]As an additional illustration, in multiuser superposition transmission (MUST), a downlink version of NOMA was proposed for the 3rd generation partnership project long-term evolution advanced (3GPP-LTE-A) initiative, where again, a two-user pairing case is considered [28], [29].

Based on 2-D HPPP statistics, the probability density function (PDF) of the distance between the RIS and its nearest BS is expressed as [30]–[32]

$$f_{r_{BR}}(x) \approx f_{r_{BU}}(x) = 2\pi\lambda_b x \exp\left(-\pi\lambda_b x^2\right). \quad (1)$$

B. RIS-aided Channel Model Design

We consider the case where the RIS has n elements, while the BSs and the users are equipped with a single antenna. The multi-antenna cases are still in our infancy and would be evaluated as future work.

For the typical NOMA pair, there are three types of communication links: i) the BU link, the direct link between the typical user and its associated BS; ii) the RU link, the link between the RIS and the typical user; and iii) the BR link, the link between its associated BS and the employed RIS. Additionally, the BR and RU links are combined as the reflecting link for the typical user. Since RISs are capable of altering the wavefront of the radio waves, the phase responses for the RIS reflect links and direct links are aligned towards the same direction. With the aid of RISs, we consider the following assumptions and definitions to fit the RIS-aided NOMA networks.

1) Small-Scale Fading Model: We assume all the links of the typical and connected users are Rayleigh fading channels[2], i.e., h_{BU} for BU links, $h_{RU,i}$ for RU links, $h_{BR,i}$ for BR links, and h_c for the links between the connected user and its BS, where $i \in [1, n]$. Hence, the PDF for Rayleigh fading channels is expressed as $f_{Rayleigh}(x) = 2x \exp\left(-x^2\right)$. Since it is assumed that the RIS is located close to the typical user, we ignore the small-scale fading for RU links.

2) Interference Analysis: Since the RIS only reflects the signals that reach its front surface, the interfering BSs are split into two portions: i) The interfering BSs reflected by the employed RIS; and ii) The interfering BSs blocked by the employed RIS. This is the key difference between RIS-aided multi-cell networks and conventional multi-cell networks. We introduce a coefficient, denoted as $\rho_I \in [0, 1]$, designed to replicate the proportion of interfering BSs augmented by RISs. Drawing from the characteristics of HPPPs, a notable observation emerges: when we envision the RIS segmenting the area into two equal sub-regions, fewer than half of the BSs are likely to impact users due to the RIS's ability to concentrate signals in particular directions. This insight naturally leads us to the conclusion that ρ_I is constrained within the range $\rho_I \leq 0.5$.

3) Path Loss Model: For each NOMA pair, the path loss model for the three links is defined as per conventional wireless communication models. Therefore, the path loss expressions for the connected user and the typical user are as

[2]We consider Rayleigh fading to depict a rich scattering environment and we also extend the channel model in terms of a general Nakagami-m fading in section III.

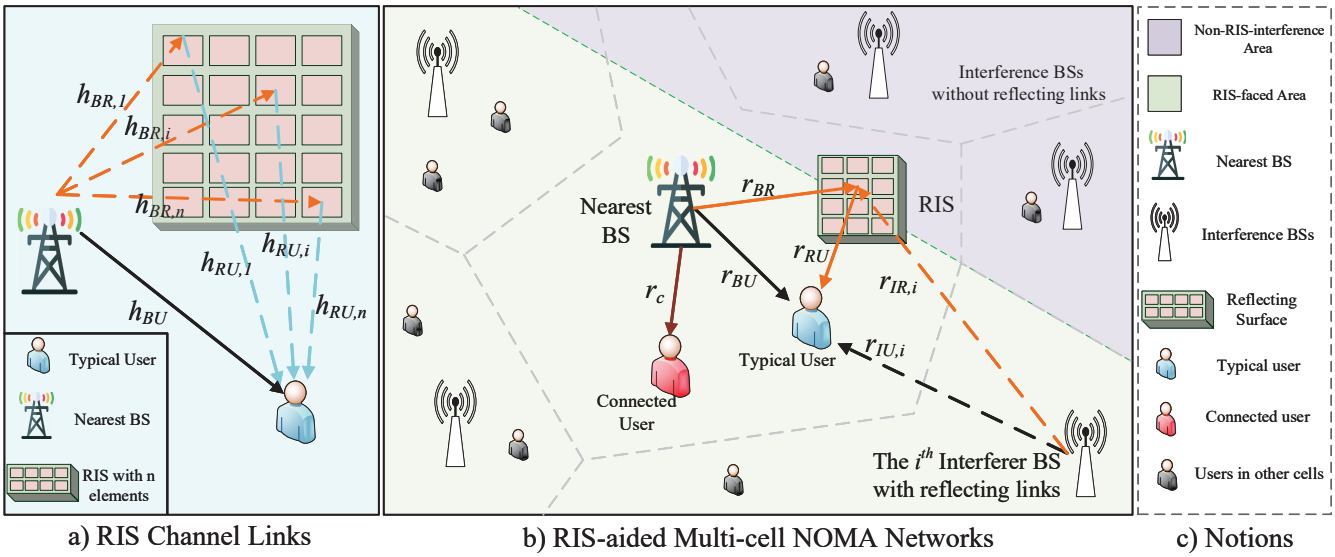

Fig. 1. Illustration of the considered signal model: (a) RIS-aided channel links with n elements: the direct and reflecting links; (b) RIS-aided multi-cell NOMA networks: a NOMA pair including a randomly distributed typical user and a connected user; (c) Legend.

follows:

$$\mathcal{P}_{BR}(\mathbf{x}_{B,near}, \mathbf{x}_R) = C_{BR} \left|\mathbf{x}_{B,near} - \mathbf{x}_R\right|^{-\alpha_t}, \quad (2)$$

$$\mathcal{P}_{RU}(O, \mathbf{x}_R) = C_{RU} \left|\mathbf{x}_R\right|^{-\alpha_t}, \quad (3)$$

$$\mathcal{P}_{BU}(O, \mathbf{x}_{B,near}) = C_{BU} \left|\mathbf{x}_{B,near}\right|^{-\alpha_t}, \quad (4)$$

$$\mathcal{P}_{c}(\mathbf{x}_{B,near}, \mathbf{x}_C) = C_{c} \left|\mathbf{x}_{B,near} - \mathbf{x}_C\right|^{-\alpha_c}, \quad (5)$$

where the $\{C_{BR}, C_{RU}, C_{BU}, C_c\} = \left(\frac{c}{4\pi f_c}\right)^2$ are reference-distance based intercepts for different links with the reference distance $d_0 = 1$ m in this work, where $c = 3 \times 10^8$ m/s is the speed of light and f_c is the used carrier frequency. The α_c is the path loss exponent for the connected user and α_t is the path loss exponent for the typical user (including the direct and reflecting links). Since the connected user is associated in the previous user association phase, $r_c = |\mathbf{x}_{B,near} - \mathbf{x}_C|$ is a constant. As the RIS is located close to the typical user and the small-scale fading for RU links is assumed as a constant, we express $|h_{RU,i}|^2 \mathcal{P}_{RU}(O, \mathbf{x}_R) = A$.

C. Signal Model

We assume that BSs possess knowledge of users' QoS demands, allowing the segregation of delay-sensitive users from delay-tolerant users. This paper employs QoS-based SIC [33]. Based on the QoS-based SIC, the messages of delay-sensitive users are detected first to avoid further latency caused by the SIC process.

In a specific case featuring a delay-sensitive near user (referred to as the connected user) coupled with a delay-tolerant far user (referred to as the typical user). To ensure quality of service based on latency, the far user has the SIC process, which may cause severe outage due to its low received power. To address this, RISs are harnessed to enhance the typical user's channel quality, thereby amplifying the SIC success rate. By utilizing QoS-based NOMA, the associated BS allocates higher transmit power to the connected user, performing SIC at the typical user to mitigate channel quality discrepancies.

The channels between the typical user and its associated BS are divided into two components: i) the reflective links via RISs; and ii) the direct link using conventional wireless communication methods. Passive beamforming designs at the RISs involve two directions: i) one to maximize received power; and ii) the other to minimize interference through signal cancellation [34]. This paper aims to improve the typical user's performance using RISs, assuming a scenario of perfect coherence achieved by appropriate passive beamforming designs. This coherence implies that all channels are aligned with the same phase, allowing signals from various links, including reflective and direct links, to be coherent with the same frequency and waveform.

With respect to the channel matrixes, we have $G_{BU} = h_{BU}\sqrt{\mathcal{P}_{BU}(O, \mathbf{x}_{B,near})}$, $\mathbf{G_{RU}} = \mathbf{H_{RU}}\sqrt{\mathcal{P}_{RU}(O, \mathbf{x}_R)}$, $\mathbf{G_{BR}} = \mathbf{H_{BR}}\sqrt{\mathcal{P}_{BR}(\mathbf{x}_{B,near}, \mathbf{x}_R)}$, and $\mathbf{G_{BR,I}} = \mathbf{H_{BR}}\sqrt{\mathcal{P}_{BR}(\mathbf{x}_I, \mathbf{x}_R)}$. We note that $\mathbf{H_{BR}} \triangleq [h_{BR,1}, h_{BR,2}, \cdots, h_{BR,n}]^T$ is the $n \times 1$ channel gain matrix of BR links, $\mathbf{x}_I$ represents the locations of interfering BSs, $\mathbf{H_{RU}} \triangleq [h_{RU,1}, h_{RU,2}, \cdots, h_{RU,n}]$ is the $1 \times n$ channel gain matrix of RU links, and $\mathbf{\Theta} \triangleq diag[\beta_1\phi_1, \beta_2\phi_2, \cdots, \beta_n\phi_n]$ is the diagonal matrix, where $\beta_n \in [0, 1]$ represents the energy loss coefficient of RISs, $\phi_n = \exp(j\theta_n)$ with $j = \sqrt{(-1)}$, and $\theta_n \in [0, 2\pi)$.

We denote an equivalent channel between the typical user and its BS as $g_{BU} = \mathbf{G_{RU}}\mathbf{\Theta}\mathbf{G_{BR}} + G_{BU}$. As for the Rayleigh variables in the complex form, we denote the smallscale fading coefficients as $h_{BR,i} = c_{BR,i} \exp(-j\theta_{BR,i})$ with $i \in [1, n]$ and $h_{BU} = c_{BU} \exp(-j\theta_{BU})$. With the assumption that the RISs are deployed near to the typical user, we consider the small-scale fading for RU links as a constant, denoted as $|h_{RU,i}|^2 \mathcal{P}_{RU}(O, \mathbf{x}_R) = A$. Based on the equations above, we simplify the equivalent channel model g_{BU} as (6) in

the next page, where ϑ_i is the initial phase of the i^{th} link, f_{BU} is the small-scale fading for the RIS-aided channel, $\mathcal{P}_{BR}\left(\mathbf{x}_{B,\text{ near}}, \mathbf{x}_R\right) = \mathcal{P}_{BU}\left(O, \mathbf{x}_{B,\text{ near}}\right) = C_t d_t^{-\alpha_t}$ for the path loss, C_t is the intercept and d_t is the distance between the typical user and its BS, which has the PDF as (1).

Based on the assumption of the perfect coherent scenario, the phases of all links are adjusted as the result of $\vartheta_i + \theta_{BR,i} = \theta_{BU} = \theta$ for all $i \in [1, n]$. Hence, we express the equivalent channel model in the power domain as

$$\left|g_{BU}\right|^2 = C_t d_t^{-\alpha_t} \left(\sum_{i=1}^{n} A \beta_i c_{BR,i} + c_{BU} \right)^2 \tag{6}$$

Therefore, the signal-to-interference-plus-noise ratio (SINR) of the SIC process at the typical user is given by

$$\begin{aligned} \gamma_{\text{SIC}} &= \frac{a_c P_t \left|\mathbf{G_{RU}} \mathbf{\Theta} \mathbf{G_{BR}} + G_{BU}\right|^2}{a_t P_t \left|\mathbf{G_{RU}} \mathbf{\Theta} \mathbf{G_{BR}} + G_{BU}\right|^2 + I_{t,\rho_I} + \sigma^2} \\ &= \frac{a_c P_t \left|g_{BU}\right|^2}{a_t P_t \left|g_{BU}\right|^2 + I_{t,\rho_I} + \sigma^2}, \end{aligned} \tag{7}$$

where

$$\begin{aligned} I_{t,\rho_I} =& \rho_I \sum_{\mathbf{x}_I \in \Phi_b \setminus \mathbf{x}_{B,\text{near}}} P_t \left|g_{BU}\right|^2 \\ &+ (1 - \rho_I) \sum_{\mathbf{x}_I \in \Phi_b \setminus \mathbf{x}_{B,\text{near}}} P_t \left|h_{BU}\right|^2 \mathcal{P}_{BU}\left(O, \mathbf{x}_I\right), \end{aligned} \tag{8}$$

with $\mathcal{P}_{BU}(O, \mathbf{x}_I) = C_{BU} \left|\mathbf{x}_I\right|^{-\alpha_t}$, a_c and a_t are the power allocation parameters for the connected and the typical user, P_t is the transmit power of BSs in NOMA pairs and σ^2 is the variance of additive white Gaussian noise (AWGN). Additionally, we set $a_c > a_t$ and $a_c + a_t = 1$. Regarding the interference I_{t,ρ_I}, we assume $\rho_I = 0.5$ to simplify the derivations, which is the maximum interference case, while the practical value is much lower than 0.5.

With the help of the SIC process, the messages from the connected user are canceled, and then the data for the typical user is decoded. The SINR after the SIC process for the typical user is expressed as:

$$\gamma_t = \frac{a_t P_t \left|\mathbf{G_{RU}} \mathbf{\Theta} \mathbf{G_{BR}} + G_{BU}\right|^2}{I_{t,\rho_I} + \sigma^2} = \frac{a_t P_t \left|g_{BU}\right|^2}{I_{t,\rho_I} + \sigma^2}. \tag{9}$$

The connected user enables to directly decode its messages by regarding the other NOMA user's signal as interference[3]. Hence, we express the SINR for the connected user as

$$\gamma_{\text{c}} = \frac{a_c P_t \left|h_c\right|^2 \mathcal{P}_c(\mathbf{x}_{B,near}, \mathbf{x}_C)}{a_t P_t \left|h_c\right|^2 \mathcal{P}_c(\mathbf{x}_{B,near}, \mathbf{x}_C) + I_c + \sigma^2}, \tag{10}$$

where $I_c = \sum_{\mathbf{x}_I \in \Phi_b \setminus \mathbf{x}_{B,near}} P_t \left|h_c\right|^2 \mathcal{P}_c(\mathbf{x}_I, \mathbf{x}_C)$ and $\mathcal{P}_c(\mathbf{x}_I, \mathbf{x}_C) = C_c \left|\mathbf{x}_I - \mathbf{x}_C\right|^{-\alpha_c}$.

D. Channel Models with "N-Fold Convolution" Method

The N-fold convolution model is an outgrowth of the traditional convolution model, which is a mathematical framework devised to tackle weighted summation across multiple variables, as outlined by equations (4) and (5) in [36]. The parameter "N" designates the number of variables involved in the convolution, leading to the designation of this model as the "N-fold convolution model"[4].

Theorem 1. *Since we consider the sub-links, including the reflecting links through each RIS element and the direct links, are independent Rayleigh fading channels, c_{BU} and $c_{BR,i}$ (for $i \in [1, n]$) are $n+1$ independent and identically distributed (i.i.d.) variables. We assume the energy loss coefficients for all RIS elements are the same, denoted as $\beta_1 = \beta_2 = \cdots = \beta_n = \beta$. Hence, the distribution of the channel model $\left|g_{BU}\right|^2$ in power domain is derived as*

$$f_{\left|g_{BU}\right|^2}(x) = \frac{1}{2\Lambda\sqrt{\frac{x}{\Lambda}}} \mathcal{L}_{S_k}^{-1} \left\{ \left(\frac{1}{2} \Psi\left(1, \frac{1}{2}; \frac{s^2}{4}\right) \right)^K \right\} \left(\sqrt{\frac{x}{\Lambda}} \right), \tag{11}$$

where $\Lambda = C_t d_t^{-\alpha_t} (A\beta)^2$ and $K = n + 1$. Additionally, $\mathcal{L}_{S_k}^{-1}\{x\}(y)$ is inverse Laplace transform of x with variable y, $\Psi(\cdot, \cdot; \cdot)$ is Tricomi's confluent hypergeometric function, and $\Psi\left(1, \frac{1}{2}; z\right) = 2 - 2\exp(z)\sqrt{\pi}\sqrt{z}\text{erfc}(\sqrt{z})$ is a special case for Tricomi's function.

Proof: See Appendix A. ∎

Since the inverse Laplace transform of $\left(\frac{1}{2}\Psi\left(1, \frac{1}{2}; \frac{s^2}{4}\right)\right)^K$ is tough to be obtained in **Theorem 1**, we cannot derive an efficient and concise distribution. Hence, we derive the asymptotic expression of the cumulative distribution function (CDF) of g_{BU} as the following corollary.

Corollary 1. *With the assumptions, i.e., $s \to \infty$ and $x \to 0^+$, the asymptotic PDF and CDF expressions of the combined channel $\left|g_{BU}\right|^2$ are derived as*

$$f_{\left|g_{BU}\right|^2}^{asy}(x) = \frac{(2x)^{K-1}}{\Lambda^K \Gamma(2K)}, \tag{12}$$

$$F_{\left|g_{BU}\right|^2}^{asy}(x) = \frac{2^{K-1} x^K}{K \Lambda^K \Gamma(2K)}. \tag{13}$$

Proof: Also see Appendix A. ∎

Remark 1. *In rural areas, we omit interference from interference BSs and define the outage probability for a BS-to-user channel as: $P_{out}^{sin}(x) = F_{\left|g_{BU}\right|^2}^{asy}\left(\frac{C_{Ra}}{\rho}\right)$, where C_{Ra} is the combined coefficient (including the transmit power and large-scale fading) and $\rho = \frac{P_t}{\sigma^2}$. Hence, the accurate diversity order via the "N-Fold Convolution" method is calculated as*

$$d_{BU}^{Ra} = -\lim_{\rho \to \infty} \frac{\log\left(F_{\left|g_{BU}\right|^2}^{asy}\left(\frac{C_{Ra}}{\rho}\right)\right)}{\log \rho} = K. \tag{14}$$

Corollary 2. *We also extend **Corollary 1** to Nakagami-m fading channels. When $s \to \infty$ and $x \to 0^+$, the asymptotic*

[3]The connected user is located beyond the LoS ball centered around the RIS [35]. As a result, any interference that might be reflected from the RISs is disregarded.

[4]The paper [37] has also exploited the "N-fold convolution model". The difference is that this paper evaluates the traditional RIS by exploiting stochastic geometry models to evaluate the spatial effect of the system, while the reference [37] evaluates another type of the RIS, which is called simultaneous transmitting and reflecting intelligent omini-surfaces.

PDF and CDF expressions are derived as

$$f_{|g_{BU}|^2}^{naka,asy}(x) = \left(\frac{2m^m\Gamma(2m)}{\Gamma(m)}\right)^K \frac{x^{mK-1}}{2\Lambda^{mK}\Gamma(2mK)}, \quad (15)$$

$$F_{|g_{BU}|^2}^{naka,asy}(x) = \left(\frac{2m^m\Gamma(2m)}{\Gamma(m)}\right)^K \frac{x^{mK}}{2mK\Lambda^{mK}\Gamma(2mK)}. \quad (16)$$

Proof: See Appendix B. ■

Remark 2. *With the same assumptions and settings in **Remark 1**, introducing C_{Na} as the combined coefficient including transmit powers and large-scale fading, the accurate diversity order under Nakagami-m fading channels is derived as*

$$d_{BU}^{Na} = -\lim_{\rho\to\infty} \frac{\log\left(F_{|g_{BU}|^2}^{naka,asy}\left(\frac{C_{Na}}{\rho}\right)\right)}{\log\rho} = mK. \quad (17)$$

Remark 3. *Based on **Remark 1** and **Remark 2**, we conclude that the diversity gains are influenced by the channel models, such as Rayleigh fading or Nakagami-m fading.*

E. Channel Models with "Curve Fitting" Tools

Since the "N-Fold Convolution" model is generally used to derive diversity gains and is difficult to obtain closed-form distribution functions, we utilize Matlab's curve fitting tools to derive a tractable expression for the RIS-aided multi-cell NOMA networks. Based on simulation results, the trend of the CDF for the channel distribution in the power domain closely approximates a Gamma distribution. Hence, we employ a Gamma distribution to fit the targeted RIS-aided channel as **Theorem 2** [38].

Our mathematical approach differs from the current research using the Gamma distribution. In the current papers, since the distribution of the product of two "i.i.d Rayleigh random variables" follows a Gamma distribution [39], they commonly use a method called "moment-matching", which calculates certain parameters of a channel model by evaluating the expectations and variations of matrices [40], [41]. Although this method has strong mathematical foundations, it becomes complex and might not provide tractable derivations when dealing with correlations or multi-cell scenarios.

In contrast, our curve fitting model offers more flexibility for different distributions and scenarios. Even though we fitted the channel as a Gamma distribution in this treatise, our model allows for other suitable distributions as well. Essentially, our approach provides more adaptability and options for modeling the channel.

Theorem 2. *The distribution for the RIS-aided channel model, including the direct and reflecting links, is fitted as a Gamma distribution. Therefore, the PDF and CDF for the small-scale fading model $|g_{BU}|^2$ in the power domain are expressed as:*

$$f_{|g_{BU}|^2}(x) = \frac{x^{a-1}}{\Gamma(a)\,b^a}\exp\left(-\frac{x}{b}\right), \quad (18)$$

$$F_{|g_{BU}|^2}(x) = \frac{\gamma(a, x/b)}{\Gamma(a)}, \quad (19)$$

where a and b are curve fitting coefficients with $a = K$, the scale coefficient $b \approx K$ when $\beta = 1$, and $\Gamma(\cdot)$ is complete gamma function and $\gamma(\cdot,\cdot)$ is the lower incomplete gamma function, denoted as $\gamma(s,x) = \int_0^x t^{s-1}e^{-t}dt$.

Remark 4. *For several specific settings, we utilizing curve fitting to calculate the coefficients as: i) $a = 5$ and $b = 4.134$ for $K = 5$ and $A = 1$; ii) $a = 5$ and $b = 2.909$ for $K = 5$ and $A = 0.8$; iii) $a = 10$ and $b = 8.041$ for $K = 10$ and $A = 1$; and iv) $a = 10$ and $b = 5.421$ for $K = 10$ and $A = 0.8$. Hence, we conclude that for our RIS-aided NOMA networks, we have the coefficient $a = K$, the scale coefficient $b \approx K$ when $\beta = 1$, which is mathematically proved as a lower bound in **Lemma 1** of [42].*

Corollary 3. *To extend the channel model of $|g_{BU}|^2$ to Nakagami-m fading channels, the PDF and CDF expressions are expressed as*

$$f_{|g_{BU}|^2}^{naka}(x) = \frac{cx^{a-1}}{\Gamma(a)\,b^a}\exp\left(-\frac{x}{b}\right)\left(\frac{\gamma(a, x/b)}{\Gamma(a)}\right)^{c-1}, \quad (20)$$

$$F_{|g_{BU}|^2}^{naka}(x) = \left(\frac{\gamma(a, x/b)}{\Gamma(a)}\right)^c, \quad (21)$$

where a, b and c are curve fitting coefficients with $a = K$. Other coefficients are obtained by curve fitting tools.

When we ignore the interference, the central limit theorem provides approximate expressions for RIS-aided systems while it is hard to obtain accurate diversity orders. Additionally, the central limit theorem cannot fit the channel models of RIS-aided networks with a few RIS elements. The derivation of "N-fold convolution" as **Theorem 1** is exploited to analyze the accurate diversity orders for RIS-aided systems. When considering stochastic geometry models, the two approaches are not friendly for multi-cell scenarios when considering interference to obtain tractable derivations, thereby we propose curve fitting models as **Theorem 2** to investigate multi-cell RIS-aided systems. We compare the channel models and present diversity orders by the following two figures (Fig. 2 and Fig. 3). The pros and cons of the mentioned three channel models are summarized by Table. I[5].

III. Performance Evaluation

Regarding performance metrics, while bit error rate (BER) hones in on individual signal transmission accuracy, coverage probability evaluates the system's capability to offer dependable communication coverage across a specified geographic area. Given our use of a stochastic geometry model and the inherent spatial unpredictability in our communication network, coverage probability becomes a more relevant and meaningful performance metric. It allows us to gauge how well our system sustains signal quality and connectivity across diverse regions, factoring in real-world elements like signal fading and interference. In essence, prioritizing coverage probability grants us insights into the overall effectiveness of our communication system's coverage abilities within an unpredictable and long-term environment.

[5]The channel models in this paper are proposed for the user served by a single RIS. When other practical scenarios are considered, multiple RISs may serve a single user or multiple users may share a single RIS, which needs further investigation of their channel models.

TABLE I
THE COMPARISON OF THREE CHANNEL MODELS

Channel models	Complexity	Accuracy	Limit
Central limit theorem	Medium	Accurate for large RIS elements	No correct diversity order
N-fold convolution	High	Accurate for high transmit SNR	No exact closed-form channel model
Curve fitting	Low	High accuracy	No theoretical proof

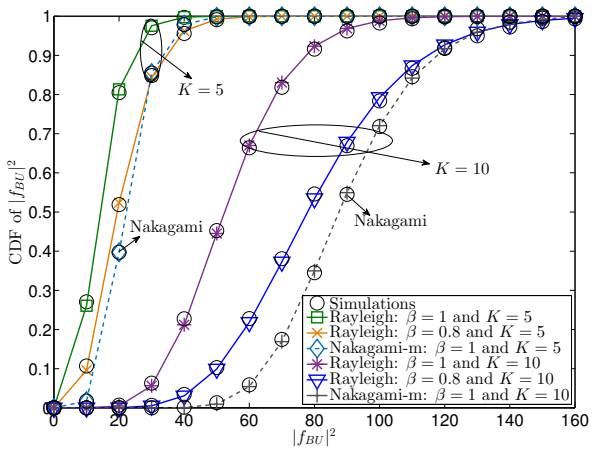

Fig. 2. The CDF versus the value of $|f_{BU}|^2$ with various numbers of RIS elements and energy loss coefficients.

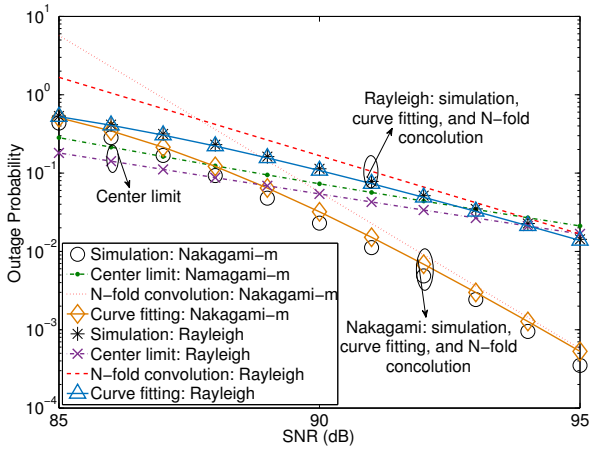

Fig. 3. (Comparison on outage performance among the central limit theorem, the N-fold convolution model, and the curve fitting model when $K = 2$, the path loss as 1000^{-3}, the outage threshold as one, the transmit power varies within $[-5, 5]$ dBm, and the noise power as -90 dB.

We're examining the coverage performance of both the typical and connected users in this section. The expression for the coverage probability of these two users is formulated as:

$$\mathrm{P}_{cov,t} = \Pr\left\{\gamma_{\mathrm{SIC}} > \gamma_{\mathrm{SIC}}^{th}, \gamma_t > \gamma_t^{th}\right\}, \tag{22}$$

$$\mathrm{P}_{cov,c} = \Pr\left\{\gamma_{\mathrm{c}} > \gamma_{\mathrm{c}}^{th}\right\}, \tag{23}$$

where $\gamma_{\mathrm{SIC}}^{th}$, γ_t^{th} and γ_{c}^{th} are the SIC threshold and coverage threshold, respectively.

A. Interference Analysis

Before delving into the performance analysis, we derive the Laplace transforms of the interference for the typical and connected users using **Lemma 1** and **Lemma 2**. For the typical user, we assume that only the interfering BSs facing the RISs possess RIS-aided channels. This categorizes the interfering BSs into two groups: i) those facing the RISs with RIS-aided channels, and ii) those located behind the RISs, using conventional wireless communication channels (Rayleigh fading channels). On the other hand, for the connected user, the interfering BSs experience Rayleigh fading channels without the aid of RISs.

Lemma 1. *For the typical user, the Laplace transform of interference, including two portions of interfering BSs, is derived as*

$$\mathcal{L}_{(s)}^{t} = \exp\left(-\pi\lambda_b d_t^2 \left({}_2F_1\left(-\frac{2}{\alpha_t}, 1; 1-\frac{2}{\alpha_t}; -\xi_1 s\right) - 1\right)\right) \times \exp\left(-\pi\lambda_b d_t^2 \left({}_2F_1\left(-\frac{2}{\alpha_t}, a; 1-\frac{2}{\alpha_t}; -\xi_2 s\right) - 1\right)\right), \tag{24}$$

where $\xi_1 = \frac{(1-\rho_I)P_t C_t}{d_t^{\alpha_t}}$, $\xi_2 = \frac{b\rho_I P_t C_t}{d_t^{\alpha_t}}$ *and* ${}_2F_1(\cdot,\cdot;\cdot;\cdot)$ *is the hypergeometric function.*

Proof: See Appendix C. ■

Lemma 2. *For the connected user, the Laplace transform of interference is derived as*

$$\mathcal{L}_{(s)}^{c} = \exp\left(-\pi\lambda_b r_c^2 \left({}_2F_1\left(-\frac{2}{\alpha_c}, 1; 1-\frac{2}{\alpha_c}; -\xi_3 s\right) - 1\right)\right), \tag{25}$$

where we have $\xi_3 = \frac{sP_t C_c}{r_c^{\alpha_c}}$.

Proof: The proof process is similar to that in ***Lemma 1*** *and we omit it here.* ■

B. Coverage Probability

Based on the derivations of the Laplace transform, we derive the coverage probability expressions for both the typical user and the connected user as follows.

Theorem 3. *Since the RISs enhance the channel quality of the typical user, we arrange for the typical user to complete*

the SIC procedure. Hence, the coverage probability following the SIC process is derived as:

$$\mathrm{P}_{cov,t} = 2\pi\lambda_b \sum_{k=1}^{a} (-1)^{k+1} \binom{a}{k} I_1, \tag{26}$$

where $I_1 = \int_0^\infty x \exp\left(-\Xi_2 x^{\alpha_t}\right) \exp\left(-\Xi_1 x^2\right) dx$, $\Upsilon = \max\left(\frac{\gamma_{\mathrm{SIC}}^{th}}{\left(a_c - \gamma_{\mathrm{SIC}}^{th} a_t\right)}, \frac{\gamma_t^{th}}{a_t}\right)$, $\Xi_2 = \frac{k\eta_t \Upsilon \sigma^2}{P_t C_t}$ *and* Ξ_1 *is expressed as*

$$\Xi_1 = \pi\lambda_{b2} F_1\left(-\frac{2}{\alpha_t}, 1; 1-\frac{2}{\alpha_t}; -k\eta_t \Upsilon\left(1-\rho_I\right)\right) + \pi\lambda_b \left({}_2F_1\left(-\frac{2}{\alpha_t}, a; 1-\frac{2}{\alpha_t}; -k\eta_t b \Upsilon \rho_I\right) - 1\right). \tag{27}$$

Proof: After we define a coefficient, denoted as $\Upsilon = \max\left(\frac{\gamma_{\mathrm{SIC}}^{th}}{\left(a_c - \gamma_{\mathrm{SIC}}^{th} a_t\right)}, \frac{\gamma_t^{th}}{a_t}\right)$*, the coverage probability is expressed as* $\mathrm{P}_{cov,t} = \Pr\left\{|f_{BU}|^2 > \Upsilon d_t^{\alpha_t}\left(I_{t,\rho_I} + \sigma^2\right)/P_t C_t\right\}$*. By exploiting the close boundary of the Gamma distribution, denoted as* $\mathrm{P}_{|f_{BU}|^2}\left\{|f_{BU}|^2 < x\right\} \approx \left(1 - \exp(-\eta_t x)\right)^N$ *with* $\eta_t = \frac{1}{b}(a!)^{-\frac{1}{a}}$ *[43], the expression of the coverage probability is derived as*

$$\mathrm{P}_{cov,t} = \sum_{k=1}^{a} (-1)^{k+1} \binom{a}{k} \mathrm{E}\left[e^{\frac{-k\eta_t \Upsilon d_t^{\alpha_t}}{P_t C_t} I_{t,\rho_I}}\right] \mathrm{E}\left[e^{\frac{-k\eta_t \Upsilon d_t^{\alpha_t} \sigma^2}{P_t C_t}}\right] = \sum_{n=1}^{a} (-1)^{k+1} \binom{a}{k} \mathrm{E}\left[e^{-\frac{k\eta_t \Upsilon d_t^{\alpha_t} \sigma^2}{P_t C_t}}\right] \mathcal{L}_{(s)}^t\left(\frac{k\eta_t \Upsilon d_t^{\alpha_t}}{P_t C_t} I_{t,\rho_I}\right), \tag{28}$$

and substituting the Laplace transform of interference for the typical user into the coverage probability expression, this theorem is proved. ∎

Corollary 4. When we consider a special case with $\alpha_t = 2$, the closed-form coverage probability expression is derived as

$$\mathrm{P}_{cov,t} = \sum_{k=1}^{a} (-1)^{k+1} \binom{a}{k} \frac{\pi\lambda_b}{\left(\Xi_1 + \Xi_2\right)}, \tag{29}$$

Proof: Based on Eq.[2.3.3.1] in [44], one is derived as

$$\begin{aligned} I_1 &= \int_0^\infty x \exp\left(-\Xi_2 x^{\alpha_t}\right) \exp\left(-\Xi_1 x^2\right) dx \\ &= \int_0^\infty \frac{1}{2} \exp\left(-\left(\Xi_1 + \Xi_2\right) t\right) dt \\ &= \frac{1}{2\left(\Xi_1 + \Xi_2\right)}, \end{aligned} \tag{30}$$

and substituting I_1 *into* (26)*, this proof ends.* ∎

Corollary 5. Conditioned on $\alpha_t = 4$, we derive the closed-form expression of the coverage probability for the typical user as

$$\mathrm{P}_{cov,t} = \sum_{k=1}^{a} \frac{\pi\lambda_b \binom{a}{k}}{2(-1)^{k+1}} \sqrt{\frac{\pi}{\Xi_2}} \exp\left(\frac{\Xi_1^2}{4\Xi_2}\right) \mathrm{erfc}\left(\frac{\Xi_1}{2\sqrt{\Xi_2}}\right), \tag{31}$$

Proof: With the aid of Eq.[2.3.15.4] in [44], we derive I_1 *as*

$$\begin{aligned} I_1 &= \int_0^\infty x \exp\left(-\Xi_2 x^4\right) \exp\left(-\Xi_1 x^2\right) dx \\ &= \frac{1}{4}\sqrt{\frac{\pi}{\Xi_2}} \exp\left(\frac{\Xi_1^2}{4\Xi_2}\right) \mathrm{erfc}\left(\frac{\Xi_1}{2\sqrt{\Xi_2}}\right), \end{aligned} \tag{32}$$

and substituting I_1 *into* (26)*, we obtain the final answer.* ∎

Theorem 4. Since the channel quality of the connected user is lower than that of the typical user, the signal of the connected user will be directly decoded to ensure its performance. Thus, the coverage probability of the connected user is derived as:

$$\mathrm{P}_{cov,c} = \exp\left(-\Xi_3 r_c^{\alpha_c}\right) \exp\left(-\Xi_4 r_c^2\right), \tag{33}$$

where $\Xi_4 = \pi\lambda_b \left({}_2F_1\left(-\frac{2}{\alpha_c}, 1; 1-\frac{2}{\alpha_c}; -\frac{\eta_c \gamma_c^{th}}{a_c - \gamma_c^{th} a_t}\right) - 1\right)$, $\Xi_3 = \eta_c \gamma_c^{th} \sigma^2 / \left(\left(a_c - \gamma_c^{th} a_t\right) P_t C_c\right)$ and $\eta_c = 1$.

Proof: The proof process is similar to that of ***Theorem 3*** *and we omit is here.* ∎

C. Asymptotic Analysis

We evaluate the asymptotic coverage performance of the NOMA users and examine the individual influence of various variables on the coverage probability for these users

1) Evaluation on $P_t \to \infty$ *:* We first investigate the asymptotic performance as the transmit power tends to infinity, denoted as $P_t \to \infty$. Hence, we derive the asymptotic coverage probability expressions by exploiting the Taylor series expansion of the exponential function, denoted as $\exp(-x) \approx 1 - x$ when $x \to 0$.

Corollary 6. Conditioned on $P_t \to \infty$, we derive the closed-form expression of the asymptotic coverage probability for the typical user as

$$\mathrm{P}_{cov,t}^{asy1} = \pi\lambda_b \sum_{k=1}^{a} (-1)^{k+1} \binom{a}{k} \left(\frac{1}{\Xi_1} - \frac{\Xi_2 \Gamma\left(\frac{\alpha_t+2}{2}\right)}{\left(\Xi_1\right)^{\frac{\alpha_t+2}{2}}}\right). \tag{34}$$

Proof: This corollary is proved by exploiting $\exp(-x) \approx 1 - x$ *and Eq.[2.3.18.2] into [44].* ∎

Corollary 7. With the assumption of $P_t \to \infty$, the closed-form expression of the asymptotic coverage probability for the connected user is derived as

$$\mathrm{P}_{cov,c}^{asy1} = \left(1 - \Xi_3 r_c^{\alpha_c}\right) \exp\left(-\Xi_4 r_c^2\right). \tag{35}$$

Proof: The proof process is similar to that of ***Corollary 6****.* ∎

Since the relationship between outage probability and coverage probability is defined as $P_{out} = 1 - P_{cov}$, we express the definition of diversity orders via $\mathrm{P}_{cov,t}^{asy1}$ and P_{cov}^{asy1} by **Remark 5**.

Remark 5. *For multi-cell scenarios considering interference from other BSs, we derive the diversity orders for the typical*

user and the connected user, respectively, as

$$d_t = -\lim_{\rho\to\infty} \frac{\log\left(1-\mathrm{P}_{cov,t}^{asy1}\right)}{\log\rho} = 0, \tag{36}$$

$$d_c = -\lim_{\rho\to\infty} \frac{\log\left(1-\mathrm{P}_{cov,c}^{asy1}\right)}{\log\rho} = 0, \tag{37}$$

where $\rho = P_t/\sigma^2$ is the transmit SNR for users.

Considering the multi-cell model, inter-cell interference becomes a factor. The derived diversity orders indicate that NOMA users exhibit diversity orders of zero. Consequently, in multi-cell scenarios, users also experience zero diversity orders. This outcome is due to amplified interference resulting from increased transmit power. Consequently, the outage performance reaches its lowest limit with zero diversity orders. These observations suggest the existence of an optimal count of RIS elements that yield the most favorable performance. However, addressing this optimization quandary is deferred to future endeavors due to constraints in available space.

2) Evaluation on $\lambda_b \to \infty$: We assume the density of BSs $\lambda_b \to \infty$, which means more BSs are allocated in this area. Hence, we analyze the asymptotic coverage probability expression of the NOMA users as the following corollaries.

Corollary 8. As for the typical user, various density of BSs λ_b influences the distributions of the associated BS and interfering BSs. Thus, with the assumption of $\lambda_b \to \infty$, the asymptotic expression is calculated as

$$\mathrm{P}_{cov,t}^{asy2} = \lim_{\lambda_b\to\infty} 2\pi\lambda_b \sum_{k=1}^{a} (-1)^{k+1} \binom{a}{k} \times \int_0^\infty x \exp\left(-\Xi_2 x^{\alpha_t}\right) \exp\left(-\Xi_1 x^2\right) = 1. \tag{38}$$

Proof: This corollary is prove by calculating the integral first and then deriving the limit. For example, when $\alpha_t = 2$, we derive $\mathrm{P}_{cov,t}^{asy2} = \lim_{\lambda_b\to\infty} \pi\lambda_b \sum_{k=1}^{a} (-1)^{k+1}\binom{a}{k} \frac{1}{\Xi_2+\Xi_1(\lambda_b)}$, where $\Xi_1(\lambda_b)$ is the function Ξ_1 with respect to λ_b. Hence, since $\lim_{x\to\infty} \frac{x}{x+C_t^{asy2}} = 1$, where C_t^{asy2} is a constant without λ_b, we can derive the final limit. Other values of α_t are calculated using similar derivations, but they are omitted here to avoid redundancy. ∎

Corollary 9. For the connected user, we consider a large λ_b with severer interference. Thus, with $\lambda_b \to \infty$, the asymptotic coverage probability is derived as

$$\mathrm{P}_{cov,c}^{asy1} = \lim_{\lambda_b\to\infty} \exp\left(-\Xi_3 r_c^{\alpha_c}\right) \exp\left(-\Xi_4 r_c^2\right) = 0. \tag{39}$$

Proof: Since $\mathrm{P}_{cov,c}^{asy1} \sim \lim_{\lambda_b\to\infty} C_{c,1}^{asy1} \exp\left(-C_{c,2}^{asy1}\lambda_b\right)$, where $C_{c,1}^{asy1}$ and $C_{c,2}^{asy1}$ are other parameters without λ_b, we calculate the limit by $\lim_{x\to\infty} \exp(-x) = 0$. ∎

Based on the evaluation of **Corollary 8** and **Corollary 9**, we conclude that increasing the number of BSs improves the coverage performance of the typical user while reducing the coverage performance for the connected user. This enhancement for the typical user occurs because employing more BSs reduces the distance between the associated BS and the typical user, consequently improving their performance. Conversely, for the connected user, the performance reduction arises due to the fixed channel condition between the associated BS and the connected user, where additional BSs amplify the strength of interference.

3) Evaluation on $n \to \infty$: We assume that the number of elements of the RISs n tends to infinity, i.e., the shape parameter a of the small-scale fading model $|f_{BU}|^2$ approaches infinity, denoted as $a \to \infty$. Since the connected user is not affected by the RISs channel parameter n, our attention is solely on the asymptotic coverage probability expression of the typical user.

Corollary 10. When we utilize large RISs, we assume RIS elements n goes to infinity to evaluate the coverage performance. Hence, the asymptotic coverage probability is derived as

$$\begin{aligned}&\mathrm{P}_{cov,t}^{asy3}\\ &=1-\lim_{a\to\infty}\left(1-2\pi\lambda_b\int_0^\infty x\exp\left(-\Xi_2 x^{\alpha_t}\right)\exp\left(-\Xi_1 x^2\right)dx\right)^a\\ &=1.\end{aligned} \tag{40}$$

Proof: This corollary is based on $1-2\pi\lambda_b\int_0^\infty x\exp\left(-\Xi_2 x^{\alpha_t}\right)\exp\left(-\Xi_1 x^2\right)dx < 1$, thereby $\lim_{a\to\infty}\left(1-2\pi\lambda_b\int_0^\infty x\exp\left(-\Xi_2 x^{\alpha_t}\right)\exp\left(-\Xi_1 x^2\right)dx\right)^a = 0$. ∎

Remark 6. *According to **Corollary 10**, the analysis demonstrates that augmenting the elements on the RISs results in enhanced coverage performance. However, larger RIS configurations might introduce more interference, potentially reducing the performance. To further examine this effect, we will assess the high Signal-to-Noise Ratio (SNR) slope of the ergodic rate in the following section.*

IV. Ergodic Rate

In this section, we derive closed-form expressions for the ergodic rates of the NOMA users. Furthermore, we evaluate the asymptotic expressions of the ergodic rate. The definitions of ergodic rates for both the typical user and the connected user are expressed as:

$$\begin{aligned}\mathrm{E}\left[R_t^{RIS}\right] &= \mathrm{E}\left[\log_2(1+\gamma_t)\right]\Pr\left\{\gamma_{\mathrm{SIC}} > \gamma_{\mathrm{SIC}}^{th}\right\}\\ &= \frac{1}{\ln 2}\int_0^\infty \frac{\mathrm{P}_{cov,t}(z)}{1+z}dz,\end{aligned} \tag{41}$$

$$\begin{aligned}\mathrm{E}\left[R_c^{RIS}\right] &= \mathrm{E}\left[\log_2(1+\gamma_c)\right]\\ &= \frac{1}{\ln 2}\int_0^\infty \frac{\mathrm{P}_{cov,c}(z)}{1+z}dz,\end{aligned} \tag{42}$$

where $\mathrm{E}[\cdot]$ is the mean value. Furthermore, in this scenario, we consider the SIC process for the typical user. Consequently, the ergodic rate of the typical user corresponds to situations where the SIC process succeeds. Therefore, if the SIC process fails, the ergodic rate becomes zero.

A. Performance Evaluation

With the help of the relationship between the derived coverage probability expressions and the definition expressions of ergodic rates shown in (41) and (42), we derive the closed-form expressions for the ergodic rates of the typical user and the connected user using the following theorems and corollaries

Theorem 5. For the typical user, the analytical expression of the ergodic rates is derived as

$$\begin{aligned}\mathrm{E}\left[R_t^{RIS}\right] = &\frac{2\pi\lambda_b}{\ln 2}\sum_{k=1}^{a}(-1)^{k+1}\binom{a}{k}\int_{a_t\Theta_c}^{\infty}\int_0^{\infty}\frac{x}{1+z}\\ &\times\exp\left(-\Theta_2(z)x^{\alpha_t}\right)\exp\left(-\Theta_1(z)x^2\right)dxdz\\ &+\frac{2\pi\lambda_b}{\ln 2}\sum_{k=1}^{a}(-1)^{k+1}\binom{a}{k}\int_0^{a_t\Theta_c}\int_0^{\infty}\frac{x}{1+z}\\ &\times\exp\left(-\frac{\Theta_2\left(a_t\Theta_c\right)}{x^{-\alpha_t}}\right)\exp\left(-\frac{\Theta_1\left(a_t\Theta_c\right)}{x^{-2}}\right)dxdz,\end{aligned} \tag{43}$$

where $\Theta_2(z)=\frac{k\eta_t z\sigma^2}{a_t P_t C_t}$, $\Theta_c=\frac{\gamma_{\mathrm{SIC}}^{th}}{\left(a_c-\gamma_{\mathrm{SIC}}^{th}a_t\right)}$ and $\Theta_1(z)=\pi\lambda_b 2F_1\left(-\frac{2}{\alpha_t},1;1-\frac{2}{\alpha_t};-k\eta_t\frac{z}{a_t}\left(1-\rho_I\right)\right)+\pi\lambda_b\left({}_2F_1\left(-\frac{2}{\alpha_t},a;1-\frac{2}{\alpha_t};-k\eta_t b\frac{z}{a_t}\rho_I\right)-1\right)$.

Proof: The detailed proof of the closed-form expressions is shown in the following corollaries. ■

Corollary 11. As for the special case of the path loss exponent $\alpha_t=2$, the closed-form expression of ergodic rates for the typical user is derived as

$$\begin{aligned}\mathrm{E}\left[R_t^{RIS}\right] = &\frac{2\pi\lambda_b}{\ln 2}\sum_{k=1}^{a}(-1)^{k+1}\binom{a}{k}\\ &\times\sum_{s=1}^{S}\frac{\omega_s\sqrt{1-v_s^2}v_s^{-2}\left(1+v_s^{-1}\right)^{-1}}{4a_t\Theta_c\left(\Theta_1\left(v_s^{-1}\right)+\Theta_2\left(v_s^{-1}\right)\right)}\\ &+\frac{2\pi\lambda_b}{\ln 2}\sum_{k=1}^{a}(-1)^{k+1}\binom{a}{k}\frac{\ln\left(a_t\Theta_c\right)}{2\left(\Theta_1\left(a_t\Theta_c\right)+\Theta_2\left(a_t\Theta_c\right)\right)},\end{aligned} \tag{44}$$

where $\omega_s=\frac{\pi}{S}$, $v_s=2a_t\Theta_c\kappa_s-1$ and $\kappa_s=\cos\left(\left(2s-1\right)\pi/\left(2S\right)\right)$.

Proof: Substituting the coverage probability expression into the definition expression of ergodic rates (41)*. Based on the equation* $\int_0^{\infty}x\exp\left(-J_2x^{\alpha_t}\right)\exp\left(-J_1x^2\right)dx=\frac{1}{2(J_1+J_2)}$*, the ergodic rate expression is derived as*

$$\begin{aligned}\mathrm{E}\left[R_t^{RIS}\right] = &\frac{2\pi\lambda_b}{\ln 2}\sum_{k=1}^{a}(-1)^{k+1}\binom{a}{k}\\ &\times\int_0^{\frac{1}{a_t\Theta_c}}\frac{t^{-2}\left(1+t^{-1}\right)^{-1}}{2\left(\Theta_1\left(t^{-1}\right)+\Theta_2\left(t^{-1}\right)\right)}dt\\ &+\frac{2\pi\lambda_b}{\ln 2}\sum_{k=1}^{a}(-1)^{k+1}\binom{a}{k}\\ &\times\frac{\ln\left(a_t\Theta_c\right)}{2\left(\Theta_1\left(a_t\Theta_c\right)+\Theta_2\left(a_t\Theta_c\right)\right)}.\end{aligned} \tag{45}$$

Exploiting Chebyshev-Gauss quadrature, which is expressed as $\int_{-1}^{+1}f(x)=\sum_{s=1}^{S}\omega_s\sqrt{1-x_s^2}\times f\left(x_s\right)$ *with* $\omega_s=\frac{\pi}{S}$ *and* $x_s=\cos\left(\left(2s-1\right)\pi/\left(2S\right)\right)$*, this corollary is proved.* ■

Corollary 12. Under the special case of the path loss exponent α_t as 4, we derive the closed-form expression of ergodic rates for the typical user as

$$\begin{aligned}\mathrm{E}\left[R_t^{RIS}\right] = &\frac{2\pi\lambda_b}{\ln 2}\sum_{k=1}^{a}(-1)^{k+1}\binom{a}{k}\sum_{s=1}^{S}\frac{\omega_s\sqrt{1-v_s^2}v_s^{-2}}{8a_t\Theta_c\left(1+v_s^{-1}\right)}\\ &\times\sqrt{\frac{\pi}{\Theta_2\left(v_s^{-1}\right)}}\exp\left(\frac{\Theta_1^2\left(v_s^{-1}\right)}{4\Theta_2\left(v_s^{-1}\right)}\right)\mathrm{erfc}\left(\frac{\Theta_1\left(v_s^{-1}\right)}{2\sqrt{\Theta_2\left(v_s^{-1}\right)}}\right)\\ &+\frac{2\pi\lambda_b}{\ln 2}\sum_{k=1}^{a}(-1)^{k+1}\binom{a}{k}\frac{\ln\left(a_t\Theta_c\right)}{4}\sqrt{\frac{\pi}{\Theta_2\left(a_t\Theta_c\right)}}\\ &\times\exp\left(\frac{\Theta_1^2\left(a_t\Theta_c\right)}{4\Theta_2\left(a_t\Theta_c\right)}\right)\mathrm{erfc}\left(\frac{\Theta_1\left(a_t\Theta_c\right)}{2\sqrt{\Theta_2\left(a_t\Theta_c\right)}}\right).\end{aligned} \tag{46}$$

Proof: Based on the integration $\int_0^{\infty}x\exp\left(-J_2x^{\alpha_t}\right)\exp\left(-J_1x^2\right)dx=\frac{1}{4}\sqrt{\frac{\pi}{J_2}}\exp\left(\frac{J_1^2}{4J_2}\right)\times\mathrm{erfc}\left(\frac{J_1}{2\sqrt{J_2}}\right)$*, the definition of ergodic rates as* (41) *and the Chebyshev-Guass quadrature, this corollary is proved and shown as the derivations in* ***Corollary 11****.* ■

Theorem 6. As for the connected user, we derive the closed-form expression of ergodic rates as

$$\begin{aligned}\mathrm{E}\left[R_c^{RIS}\right] = &\sum_{s=1}^{S}\frac{\omega_s\sqrt{1-\chi_s^2}}{\ln 2\left(1+\chi_s\right)}\exp\left(-\Theta_3\left(\chi_s\right)r_c^{\alpha_c}\right)\\ &\times\exp\left(-\Theta_4\left(\chi_s\right)r_c^2\right),\end{aligned} \tag{47}$$

where $\Theta_3(z)=\frac{\eta_c z\sigma^2}{(a_c-za_t)P_tC_c}$, $\Theta_4(z)=\pi\lambda_b\left({}_2F_1\left(-\frac{2}{\alpha_c},1;1-\frac{2}{\alpha_c};-\frac{\eta_c z}{a_c-za_t}\right)-1\right)$, and $\chi_s=\frac{a_c(\kappa_s+1)}{2a_t}$.

Proof: The proof process is similar to that of ***Theorem 5****,* ***Corollary 11****, and* ***Corollary 12****.* ■

B. Asymptotic Analysis

When we use a high transmit power of users to evaluate the coverage performance, we derive the asymptotic ergodic rate and investigate the high SNR slope for ergodic rates.

Corollary 13. Conditioned on $P_t\to\infty$, the asymptotic expression of the ergodic rate for the typical user is derived as

$$\begin{aligned}\mathrm{E}\left[R_t^{RIS}\right] = &\frac{\pi\lambda_b}{\ln 2}\sum_{k=1}^{a}(-1)^{k+1}\binom{a}{k}\sum_{s=1}^{S}\frac{\omega_s\sqrt{1-v_s^2}v_s^{-2}}{2a_t\Theta_c\left(1+v_s^{-1}\right)}\\ &\times\left(\frac{1}{\Theta_1\left(v_s^{-1}\right)}-\frac{\Theta_2\left(v_s^{-1}\right)\Gamma\left(\frac{\alpha_t+2}{2}\right)}{\left(\Theta_1\left(v_s^{-1}\right)\right)^{\frac{\alpha_t+2}{2}}}\right)\\ &+\frac{\pi\lambda_b}{\ln 2}\sum_{k=1}^{a}(-1)^{k+1}\binom{a}{k}\ln\left(a_t\Theta_c\right)\\ &\times\left(\frac{1}{\Theta_1\left(a_t\Theta_c\right)}-\frac{\Theta_2\left(a_t\Theta_c\right)\Gamma\left(\frac{\alpha_t+2}{2}\right)}{\left(\Theta_1\left(a_t\Theta_c\right)\right)^{\frac{\alpha_t+2}{2}}}\right)\end{aligned} \tag{48}$$

Proof: According to the asymptotic expression, denoted as $\exp(-x) = 1 - x$, *and the integration, denoted as* $\int_0^\infty x\left(1-\Theta_2\left(z\right)x^{\alpha_t}\right)\exp\left(-\Theta_1\left(z\right)x^2\right)dx = \frac{1}{2}\left(\frac{1}{\Theta_1(z)} - \frac{\Theta_2(z)\Gamma\left(\frac{\alpha_t+2}{2}\right)}{\left(\Theta_1(z)\right)^{\frac{\alpha_t+2}{2}}}\right)$, *the ergodic rate expression is rewritten as*

$$\begin{aligned}\mathrm{E}\left[R_t^{RIS}\right] =& \frac{\pi\lambda_b}{\ln 2}\sum_{k=1}^{a}(-1)^{k+1}\binom{a}{k}\int_{a_t\Theta_c}^{\infty}\frac{1}{1+z} \\ &\times\left(\frac{1}{\Theta_1(z)} - \frac{\Theta_2(z)\Gamma\left(\frac{\alpha_t+2}{2}\right)}{\left(\Theta_1(z)\right)^{\frac{\alpha_t+2}{2}}}\right)dz \\ &+ \frac{\pi\lambda_b}{\ln 2}\sum_{k=1}^{a}(-1)^{k+1}\binom{a}{k}\ln\left(a_t\Theta_c\right) \\ &\times\left(\frac{1}{\Theta_1\left(a_t\Theta_c\right)} - \frac{\Theta_2\left(a_t\Theta_c\right)\Gamma\left(\frac{\alpha_t+2}{2}\right)}{\left(\Theta_1\left(a_t\Theta_c\right)\right)^{\frac{\alpha_t+2}{2}}}\right).\end{aligned} \tag{49}$$

By exploiting the Chebyshev-Gauss quadrature and some numerical transformations, the final expression is derived as (48). ■

Corollary 14. With the assumption when the transmit power goes to infinity, denoted as $P_t \to \infty$, the asymptotic expression of ergodic rates for the connected user is derived as

$$\begin{aligned}\underset{\rho\to\infty}{\mathrm{E}}\left[R_c^{RIS}\right] =& \sum_{s=1}^{S}\frac{\omega_s\sqrt{1-\chi_s^2}}{\ln 2\left(1+\chi_s\right)}\left(1-\Theta_3\left(\chi_s\right)r_c^{\alpha_c}\right) \\ &\times\exp\left(-\Theta_4\left(\chi_s\right)r_c^2\right).\end{aligned} \tag{50}$$

Proof: The proof process is similar to that of ***Corollary 6***. ■

Remark 7. *When* $P_t \to \infty$ *is assumed, which means* $\lambda = P_t/\sigma^2 \to \infty$, *we express the definition of high SNR slopes for ergodic rates as*

$$S_t = \lim_{\rho\to\infty}\frac{\underset{\rho\to\infty}{\mathrm{E}}\left[R_t^{RIS}\right]}{\log\left(\rho\right)} = 0, \tag{51}$$

$$S_c = \lim_{\rho\to\infty}\frac{\underset{\rho\to\infty}{\mathrm{E}}\left[R_c^{RIS}\right]}{\log\left(\rho\right)} = 0. \tag{52}$$

Remark 8. *When* $n \to \infty$ *is assumed, which means the we equip large amounts of elements on the RISs, we express the definition of large-element slopes for the ergodic rates as*

$$S_{t,n\to\infty} = \lim_{n\to\infty}\frac{\underset{n\to\infty}{\mathrm{E}}\left[R_t^{RIS}\right]}{\log\left(n\right)} = 0. \tag{53}$$

Remark 9. *Based on* ***Remark 7*** *and* ***Remark 8****, the evaluation shows that all the slopes are zero. This implies that despite enhancing the transmit power* P_t *or using a large number of elements* n *to a large extent, the ergodic rate performance reaches an upper limit. This occurs because as the transmit power* P_t *and element number* n *improve, both the received power and interference increase, contributing to the ergodic rate's upper limit.*

Remark 10. *We exploit the energy efficiency as* $e = \frac{\textit{Egodic Rate}}{\textit{Transmit Power}}$ *to gauge the achievable transmission rate per unit transmit power. By exploiting the derived ergodic rates, we evaluate the energy efficiency as*

$$e_t = \frac{\mathrm{E}\left[R_t^{RIS}\right]}{P_t}, \tag{54}$$

$$e_c = \frac{\mathrm{E}\left[R_c^{RIS}\right]}{P_t}. \tag{55}$$

V. Numerical Results

We exploit the Monte Carlo simulation to validate analytical coverage probability for the typical user (**Theorem 3**) and the connected user (**Theorem 4**). Without otherwise specification, we set the numerical coefficients as: the noise power as $\sigma^2 = -170 + 10\log\left(f_c\right) + N_f = -90$ dB with the bandwidth f_c as 10 MHz and the noise figure N_f as 10 dB, the wave length $W = c/f_c$, the speed of light $c = 3\times10^8$ m/s, reference-distance-based intercepts as $C_{BR} = C_{RU} = C_{BU} = C_c = \left(\frac{W}{4\pi}\right)^2$, the transmit power of users P_t as $[0, 30]$ dBm, path loss exponents as $\alpha_c = \alpha_t = 4$, the density of BSs as $\lambda_b = 1/(300^2\pi)$, thresholds as $\gamma_{SIC}^{th} = \gamma_t^{th} = \gamma_c^{th} = 10^{-2}$, and power allocation coefficients $a_c = 0.6$ and $a_t = 0.4$. The number of the RIS elements n and the energy loss coefficient β is defined in the following paragraphs.

As for the OMA cases, the typical user and the connected user divide the entire spectrum resources into two portions. Since they use different spectrum resources, there is no interference between the two users. Hence, the rate expression under the OMA case can be expressed as $\frac{1}{2}\log\left(1+\mathrm{SNR}\right)$, while that for NOMA is expressed as $\log\left(1+SNR/SINR\right)$. Therefore, the simulation results will follow this design to compare the performance between OMA and NOMA networks.

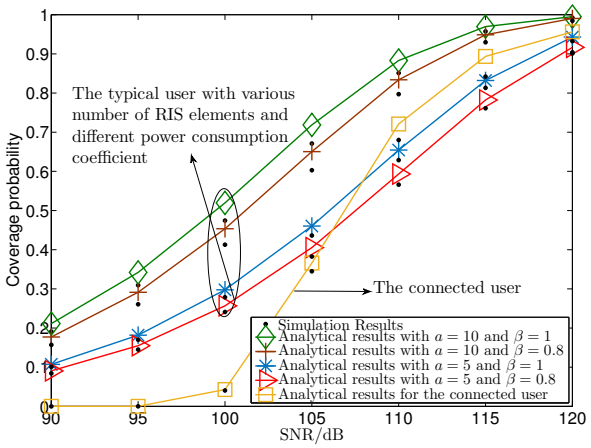

Fig. 4. Coverage probability versus transmit SNR with various numbers of RIS elements $K = a = \{5, 10\}$ and energy loss coefficients $\beta = \{1, 0.8\}$.

A. Coverage Probability

The coverage performance versus transmit SNR is investigated via Fig. 4, which demonstrates that all the analytical results are upper bounds since we utilize a close upper bound

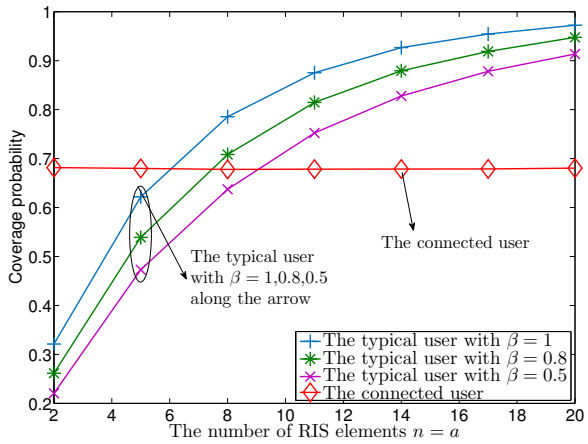

Fig. 5. Coverage probability versus the number of RIS elements with $P_t = 20$ dBm and various energy loss coefficients $\beta = \{1, 0.8\}$.

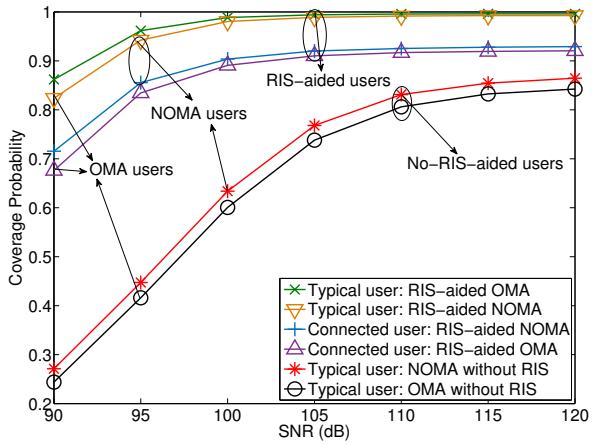

Fig. 6. Comparison on coverage probability: RIS-aided NOMA, RIS-aided OMA, NOMA without RISs, and OMA without RISs.

assumption to derive the coverage probability. One observation is that increasing the number of RIS elements and energy loss coefficient enhances the performance of the typical user. This improvement occurs because enlarging the RIS element number and reducing the power consumption improve the channel quality of the typical user.

Considering the number of RIS elements n, Fig. 5 investigates the performance variation based on n. Two observations are apparent: i) The coverage probability with a large number of RIS elements n and the energy loss coefficient β outperforms that with low n and β; ii) The RISs have no influence on the connected user as no RIS aids the connected user.

We compare the coverage performance of RIS-aided NOMA users, RIS-aided OMA users, NOMA users without RISs, and OMA users without RISs in Fig. 6. The simulation results indicate a significant improvement in the typical user's coverage performance due to RISs. By consolidating signals between the typical user and its associated BS, the channel gain of the typical user with RISs surpasses that without RISs, addressing the issue of poor performance among cell-edge users in NOMA systems. Additionally, another observation highlights that the NOMA technique enhances the coverage performance of the typical user. Through QoS-based NOMA, the typical user mitigates interference using SIC, resulting in further performance enhancement.

B. Ergodic Rate

In this subsection, we explore the ergodic sum rate of RIS-aided NOMA networks through numerical results. The coefficients and settings remain consistent with those in the subsection "coverage probability," except for specific statements. Therefore, we validate our derivations and extract several insights from simulations.

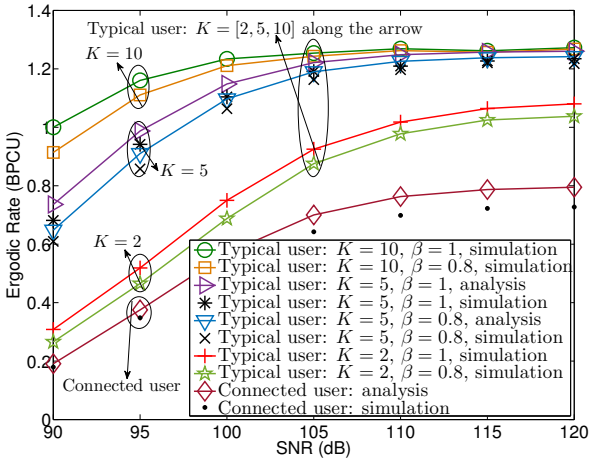

Fig. 7. Ergodic rates versus SNR with various numbers of RIS elements ($K = [2, 5, 10]$) and energy loss coefficients ($\beta = [0.8, 1]$).

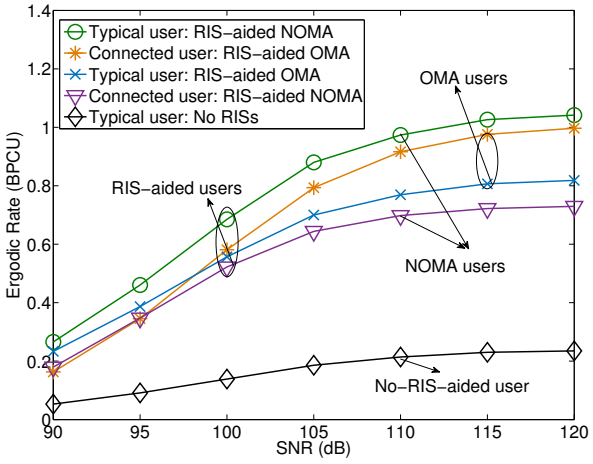

Fig. 8. The CDF versus the values of $|f_{BU}|^2$ with various numbers of RIS elements and energy loss coefficients.

We investigate the ergodic rate performance versus SNR in Fig. 7 with the unit "bit per cell use (BPCU)". Firstly, this figure validates our derivations of ergodic rates, demonstrating their proximity to the simulation results as close upper bounds.

This is due to our use of approximated expressions from the Gamma distribution to calculate user interferences. Moreover, it illustrates that the ergodic rate reaches an upper limit with increasing transmit SNR. As we enhance the transmit SNR, both received signals and interference amplify, resulting in error floors. Considering **Remark 7** to **Remark 9**, we conclude that upper limits arise in multi-cell RIS-aided NOMA networks when continually increasing transmit power or the number of RIS elements.

The ergodic rate performance of RIS-aided NOMA users, RIS-aided OMA users, and users without RISs is compared in Fig. 8. For this figure, we employ specific settings, such as setting the number of RIS elements to one ($K = n + 1 = 2$). This situation allows us to explore how a single element influences user channels. The figure demonstrates that even with just one element, RISs significantly enhance the sum rate. This observation leads us to conclude that RISs hold promise in boosting user performance. Furthermore, Fig. 8 validates that connected users experience reduced rates compared to the traditional OMA case due to interference from the typical user. However, the sum rates of all NOMA users have increased. Compared to the OMA case in a NOMA pair, the user with the SIC process has smaller ergodic rates, while the user without the SIC process has larger ergodic rates.

VI. Conclusion

This paper has investigated the coverage probability of a coherent scenario for RIS-aided multi-cell NOMA frameworks, where stochastic geometry models are exploited to capture the spatial effects of NOMA users. We have proposed two RIS-aided channel models, namely the N-fold convolution model and the curve fitting model. We have derived the asymptotic expressions using the N-fold convolution model to calculate diversity orders. Additionally, we have used curve fitting tools to investigate multi-cell networks. For Rayleigh fading channels, the RIS-aided channel model is closely modeled as a Gamma distribution. For Nakagami-m fading channels, the channel model is fitted as a power function of the Gamma distribution. Based on the two models, we have derived the outage probability and ergodic rate expressions, including closed-form approximations and asymptotic expressions. The analytical results have revealed that: i) The shape coefficient of the Gamma distribution a is equal to the number of channels K; ii) The scale coefficient b is approximately equal to n when the energy loss coefficient $\beta = 1$ holds; and iii) when the interference strength from other cells is low, the diversity order is proportional to the number of channels K. Numerical results have concluded that: i) RISs can enhance the channel quality of their aided users; ii) The performance is further improved by increasing the number of RIS elements n and the energy loss coefficient β, while the performance has upper limits; and iii) RISs provide high flexibility in decoding orders by adjusting the number of elements n. Our research findings confirm an intriguing trend in multi-cell RIS-aided NOMA networks. Specifically, we have demonstrated that a combination of the minimal count of RIS elements and the least required transmit power can lead to the attainment of maximum sum rates. This insight underscores the significance of future endeavors aimed at optimizing this promising configuration. The effect of blockages awaits analysis, making such an investigation more practical [45]. Additionally, our forthcoming investigations will explore topics such as relative interference management, power allocation, multi-antenna scenarios, and practical stochastic geometry models.

Appendix A: Proof of Theorem 1 and Corollary 1

When the number of RIS elements n is large enough, we assume the channel fading model as

$$\begin{aligned}|g_{BU}|^2 &= C_t d_t^{-\alpha_t}\left(\sum_{i=1}^{n} A\beta_i c_{BR,i} + c_{BU}\right)^2 \\ &\approx C_t d_t^{-\alpha_t}(A\beta S_K)^2, \end{aligned} \tag{A.1}$$

where we set $c_{n+1} = c_{BU}$, $c_k = c_{BR,k}$ and $S_K = \sum_{k=1}^{K} c_k$ for $K = n + 1$.

Firstly, since the K variables have the same density distributions, we briefly derive the distribution of the sum of K independent random variables, denoted as S_K. Noted that a property for the distribution of S_K is expressed as

$$\mathcal{L}_{S_K}\left[f_{S_K}(x)\right](s) = \left\{\mathcal{L}_{S_K}\left[f_{Rayleigh}(x)\right](s)\right\}^K, \tag{A.2}$$

where $f_{Rayleigh}(x)$ is the PDF of Rayleigh fading channels and $\mathcal{L}_{S_K}[x](s)$ is the Laplace transform of x with variable s. Hence, according to Eq. [2.3.15.1] in table [44], the Laplace transform of S_K is calculated as

$$\mathcal{L}_{S_K}\left[f_{S_K}(x)\right](s) = \left(\Gamma(2)\exp\left(\frac{s^2}{8}\right)D_{-2}\left(\frac{s}{\sqrt{2}}\right)\right)^K, \tag{A.3}$$

where $D_{-V}(\cdot)$ is the parabolic-cylinder function shown in the index of notions in table [44].

Additionally, a special case with special values for the parabolic-cylinder function is expressed as $D_{-2}\left(\frac{s}{\sqrt{2}}\right) = \frac{1}{2}\exp\left(-\frac{s^2}{8}\right)\Psi\left(1, \frac{1}{2}; \frac{s^2}{4}\right)$. Hence, the PDF of S_K is expressed as

$$f_{S_K}(x) = \mathcal{L}_{S_k}^{-1}\left\{\left(\frac{1}{2}\Psi\left(1, \frac{1}{2}; \frac{s^2}{4}\right)\right)^K\right\}(x). \tag{A.4}$$

When variable x with its PDF $f_x(x)$, the PDF for $y = ax^2$ is derived as $f_y(y) = \frac{1}{2a\sqrt{(y/a)}} \times \left[f_x(\sqrt{(y/a)}) + f_x(-\sqrt{(y/a)})\right]$ for $y > 0$. Hence, with the aid of the mentioned equation, the PDF of the equivalent channel model in power domain $|g_{BU}|^2 = \Lambda S_K^2$ is obtained as **Theorem 1**.

Utilizing the asymptotic expression $\Psi(a, b; z) \approx z^{-a}{}_2F_0\left(a, a - b + 1; ; -\frac{1}{z}\right)$ when $s \to \infty$, we further express the PDF of S_K as

$$f_{S_K}(x) = \mathcal{L}_{S_k}^{-1}\left\{\left[\frac{2}{s^2}{}_2F_0\left(1, 1.5; ; -\frac{4}{s^2}\right)\right]^K\right\}(x). \tag{A.5}$$

$$f_{\substack{S_k\\x\to 0^+}}^{naka}(x) \approx \mathcal{L}_{S_k}^{-1}\left\{\left(\frac{\Gamma(2m)}{2^{2m-1}\Gamma(m)}\left(\frac{s^2}{4m}\right)^{-m}{}_2F_0\left(m,m+\frac{1}{2};;-\frac{4m}{s^2}\right)\right)^K\right\}(x)$$
$$\approx \mathcal{L}_{S_k}^{-1}\left\{\left(\frac{2m^m\Gamma(2m)}{\Gamma(m)}\right)^K s^{-2mK}\right\}(x) = \left(\frac{2m^m\Gamma(2m)}{\Gamma(m)}\right)^K \frac{x^{2mK-1}}{\Gamma(2mK)}. \quad \text{(B.4)}$$

Since ${}_2F_0\left(1,1.5;;-\frac{4}{s^2}\right)=1$ when $s\to\infty$ and utilizing $\mathcal{L}\left[x^v\right](s)=\frac{\Gamma(v+1)}{s^{v+1}}$ [26], we further derive the above expression as

$$f_{S_k}^{asy}(x) = \mathcal{L}_{S_k}^{-1}\left\{\frac{2^K}{s^{2K}}\right\}(x) = \frac{2^K x^{2K-1}}{\Gamma(2K)}. \quad \text{(A.6)}$$

and the final PDF and CDF expressions for $|g_{BU}|^2=\Lambda S_K^2$ are derived as **Corollary 1**.

Appendix B: Proof of Corollary 2

Following the proof of **Theorem 1**, the Laplace transform expression of the PDF of S_k is expressed as

$$\mathcal{L}_{S_k}\left[f_{S_k}^{naka}(x)\right](s) = \left(\int_0^\infty \frac{2m^m}{\Gamma(m)}x^{2m-1}\exp\left(-mx^2\right)\exp\left(-sx\right)dx\right)^K. \quad \text{(B.1)}$$

Based on Eq.[2.3.15.3] in [44], we derive the above equation as

$$\mathcal{L}_{S_k}\left[f_{S_k}^{naka}(x)\right](s) = \left(\frac{2^{1-m}\Gamma(2m)}{\Gamma(m)}\exp\left(\frac{s^2}{8m}\right)D_{-2m}\left(\frac{s}{\sqrt{2m}}\right)\right)^K. \quad \text{(B.2)}$$

Since the parabolic-cylinder function is expressed as $D_v(z)=2^{v/2}\exp\left(-\frac{z^2}{4}\right)\Psi\left(-\frac{v}{2},\frac{1}{2};\frac{z^2}{2}\right)$, we further derive the Laplace transform of $f_{S_k}^{naka}(x)$ as

$$\mathcal{L}_{S_k}\left[f_{S_k}^{naka}(x)\right](s) = \left(\frac{\Gamma(2m)}{2^{2m-1}\Gamma(m)}\Psi\left(m,\frac{1}{2};\frac{s^2}{4m}\right)\right)^K. \quad \text{(B.3)}$$

Utilizing the asymptotic expressions $\Psi(a,b;z)\approx z^{-a}{}_2F_0\left(a,a-b+1;;-\frac{1}{z}\right)$ and ${}_2F_0(x,y;;0)=1$ when $s\to\infty$, we derive the asymptotic PDF expression $f_{S_k}^{naka}(x)$ as (B.4)

Finally, substituting (B.4) into $f_y(y)=\frac{1}{2a\sqrt{(y/a)}}\left[f_x(\sqrt{(y/a)})+f_x(-\sqrt{(y/a)})\right]$ with $y>0$ and $|g_{BU}|^2=\Lambda S_K^2$, we derive the final PDF and CDF expressions for $|g_{BU}|^2$.

Appendix C: Proof of Lemma 1

Based on the Campbells theorem, the Laplace transform expression of the interference for the typical user is derived as

$$L_{(s)}^t = \underbrace{\mathrm{E}\left[\prod_{\mathbf{x}_I\in\Phi_r\setminus\mathbf{x}_B}\exp\left(-\frac{\rho_I s P_t C_t |f_{BU}|^2}{d_I^{\alpha_t}}\right)\right]}_{I_3} \times \underbrace{\mathrm{E}\left[\prod_{\mathbf{x}_I\in\Phi_r\setminus\mathbf{x}_B}\exp\left(-\frac{s(1-\rho_I)P_t|h_{BU}|^2C_t}{d_I^{\alpha_t}}\right)\right]}_{I_2}. \quad \text{(C.1)}$$

For the derivation of I_2, the channel distribution is Rayleigh distribution as this portion is to evaluate the interference without the aid of RISs. By exploiting probability generating functional (PGFL) and $\int_A^\infty\left(1-\frac{1}{(1+sy^{-\alpha})^N}\right)ydy = \frac{A^2}{2}\left({}_2F_1\left(-\frac{2}{\alpha},N;1-\frac{2}{\alpha};-\frac{s}{A^\alpha}\right)-1\right)$, I_2 is derived as

$$I_2 = \exp\left(-\pi\lambda_b d_t^2\left({}_2F_1\left(-\frac{2}{\alpha_t},1;1-\frac{2}{\alpha_t};-\xi_1 s\right)-1\right)\right), \quad \text{(C.2)}$$

For the derivations of I_3, we evaluate the interference BSs facing the RISs, thus the equivalent channel is the Gamma distribution obtained by the curve fitting method. After exploiting the PGFL, substituting the PDF of the curve fitting model into the I_3 expression, we obtain

$$I_3 = \exp\left(-2\pi\lambda_b\int_{d_t}^\infty\left(1-\left(1+b\rho_I s P_t C_t r^{-\alpha_t}\right)^{-a}\right)rdr\right). \quad \text{(C.3)}$$

Exploiting the integration of $\int_A^\infty\left(1-\frac{1}{(1+sy^{-\alpha})^N}\right)ydy$ above, the final expression of I_3 is derived as

$$I_3 = \exp\left(-\pi\lambda_b d_t^2\left({}_2F_1\left(-\frac{2}{\alpha_t},a;1-\frac{2}{\alpha_t};-\xi_2 s\right)-1\right)\right), \quad \text{(C.4)}$$

and multiplying I_2 and I_3 to obtain the final expression of the Laplace transform for the typical user.

References

[1] C. Zhang, W. Yi, Y. Liu, and Q. Wang, "Multi-cell NOMA: Coherent reconfigurable intelligent surfaces model with stochastic geometry," *in Proc. IEEE Int. Conf. on Commun. (ICC)*, pp. 1–6, Jun. 2021.

[2] Z. Ding, X. Lei, G. K. Karagiannidis, R. Schober, J. Yuan, and V. K. Bhargava, "A survey on non-orthogonal multiple access for 5G networks: Research challenges and future trends," *IEEE J. Sel. Areas Commun.*, vol. 35, no. 10, pp. 2181–2195, Oct. 2017.

[3] W. Yi, Y. Liu, A. Nallanathan, and M. Elkashlan, "Clustered millimeter-wave networks with non-orthogonal multiple access," *IEEE Trans. Commun.*, vol. 67, no. 6, pp. 4350–4364, Jun. 2019.

[4] C. Huang, S. Hu, G. C. Alexandropoulos, A. Zappone, C. Yuen, R. Zhang, M. D. Renzo, and M. Debbah, "Holographic MIMO surfaces for 6G wireless networks: Opportunities, challenges, and trends," *IEEE Wireless Commun.*, vol. 27, no. 5, pp. 118–125, Oct. 2020.

[5] X. Mu, Y. Liu, L. Guo, J. Lin, and R. Schober, "Simultaneously transmitting and reflecting (STAR) RIS aided wireless communications," *IEEE Trans. Wireless Commun.*, vol. 21, no. 5, pp. 3083–3098, May 2022.

[6] Y. Liu, Z. Qin, M. Elkashlan, Z. Ding, A. Nallanathan, and L. Hanzo, "Nonorthogonal multiple access for 5G and beyond," *Proc. IEEE*, vol. 105, no. 12, pp. 2347–2381, 2017.

[7] M. Di Renzo, F. Habibi Danufane, X. Xi, J. de Rosny, and S. Tretyakov, "Analytical modeling of the path-loss for reconfigurable intelligent surfaces−anomalous mirror or scatterer?" *in Proc. IEEE 21th Int. Workshop Signal Process. Adv. Wireless Commun. (SPAWC)*, pp. 1–5, 2020.

[8] W. Tang, M. Z. Chen, X. Chen, J. Y. Dai, Y. Han, M. Di Renzo, Y. Zeng, S. Jin, Q. Cheng, and T. J. Cui, "Wireless communications with reconfigurable intelligent surface: Path loss modeling and experimental measurement," *IEEE Trans. Wireless Commun.*, vol. 20, no. 1, pp. 421–439, Jan. 2021.

[9] V. S. Asadchy, W. Wickberg, A. Diaz-Rubio, and M. Wegener, "Eliminating scattering loss in anomalously reflecting optical metasurfaces," *ACS Photonics*, vol. 4, no. 5, pp. 1264–1270, Apr. 2017.

[10] C. Zhang, W. Yi, Y. Liu, K. Yang, and Z. Ding, "Reconfigurable intelligent surfaces aided multi-cell NOMA networks: A stochastic geometry model," *IEEE Trans. Commun.*, vol. 70, no. 2, pp. 951–966, Feb. 2022.

[11] N. Shlezinger, G. C. Alexandropoulos, M. F. Imani, Y. C. Eldar, and D. R. Smith, "Dynamic metasurface antennas for 6G extreme massive MIMO communications," *IEEE Wireless Commun.*, vol. 28, no. 2, pp. 106–113, Apr. 2021.

[12] E. Björnson, L. Sanguinetti, H. Wymeersch, J. Hoydis, and T. L. Marzetta, "Massive MIMO is a reality - What is next?: Five promising research directions for antenna arrays," *Digital Signal Processing*, vol. 94, pp. 3–20, 2019.

[13] W. Yan, X. Yuan, Z. Q. He, and X. Kuai, "Passive beamforming and information transfer design for reconfigurable intelligent surfaces aided multiuser MIMO systems," *IEEE J. Sel. Areas Commun.*, vol. 38, no. 8, pp. 1793–1808, Aug. 2020.

[14] M. Jung, W. Saad, M. Debbah, and C. S. Hong, "On the optimality of reconfigurable intelligent surfaces (RISs): Passive beamforming, modulation, and resource allocation," *IEEE Trans. Wireless Commun.*, vol. 20, no. 7, pp. 4347–4363, Jul. 2021.

[15] B. Di, H. Zhang, L. Song, Y. Li, Z. Han, and H. V. Poor, "Hybrid beamforming for reconfigurable intelligent surface based multi-user communications: Achievable rates with limited discrete phase shifts," *IEEE J. Sel. Areas Commun.*, vol. 38, no. 8, pp. 1809–1822, Aug. 2020.

[16] R. Karasik, O. Simeone, M. D. Renzo, and S. Shamai Shitz, "Adaptive coding and channel shaping through reconfigurable intelligent surfaces: An information-theoretic analysis," *IEEE Trans. Commun.*, vol. 69, no. 11, pp. 7320–7334, Nov. 2021.

[17] C. Huang, R. Mo, and C. Yuen, "Reconfigurable intelligent surface assisted multiuser MISO systems exploiting deep reinforcement learning," *IEEE J. Sel. Areas Commun.*, vol. 38, no. 8, pp. 1839–1850, Aug. 2020.

[18] S. Khan and S. Y. Shin, "Deep-learning-aided detection for reconfigurable intelligent surfaces," Oct. 2019, arXiv preprint arXiv:1910.09136. [Online]. Available: https://arxiv.org/abs/1910.09136

[19] X. Yang, C. K. Wen, and S. Jin, "MIMO detection for reconfigurable intelligent surface-assisted millimeter wave systems," *IEEE J. Sel. Areas Commun.*, vol. 38, no. 8, pp. 1777–1792, Aug. 2020.

[20] M. Nemati, B. Maham, S. R. Pokhrel, and J. Choi, "Modeling RIS empowered outdoor-to-indoor communication in mmwave cellular networks," *IEEE Trans. Commun.*, vol. 69, no. 11, pp. 7837–7850, Nov. 2021.

[21] A. U. Makarfi, K. M. Rabie, O. Kaiwartya, O. S. Badarneh, X. Li, and R. Kharel, "Reconfigurable intelligent surface enabled IoT networks in generalized fading channels," *in Proceedings in ICC 2020*, pp. 1–6, 2020.

[22] Y. Liu, X. Mu, X. Liu, M. Di Renzo, Z. Ding, and R. Schober, "Reconfigurable intelligent surface-aided multi-user networks: Interplay between NOMA and RIS," *IEEE Wireless Commun.*, vol. 29, no. 2, pp. 169–176, Apr. 2022.

[23] T. Hou, Y. Liu, Z. Song, X. Sun, Y. Chen, and L. Hanzo, "MIMO assisted networks relying on intelligent reflective surfaces: A stochastic geometry based analysis," *IEEE Trans. Veh. Tech.*, vol. 71, no. 1, pp. 571–582, Jan 2022.

[24] Z. Ding and H. Vincent Poor, "A simple design of IRS-NOMA transmission," *IEEE Commun. Lett.*, vol. 24, no. 5, pp. 1119–1123, May 2020.

[25] Z. Ding, R. Schober, and H. V. Poor, "On the impact of phase shifting designs on IRS-NOMA," *IEEE Wireless Commun. Lett.*, vol. 9, no. 10, pp. 1596–1600, Oct. 2020.

[26] Y. Cheng, K. H. Li, Y. Liu, K. C. Teh, and G. K. Karagiannidis, "Non-orthogonal multiple access (NOMA) with multiple intelligent reflecting surfaces," *IEEE Trans. Wireless Commun.*, vol. 20, no. 11, pp. 7184–7195, Nov. 2021.

[27] T. Wang, G. Chen, M.-A. Badiu, and J. P. Coon, "Performance analysis of RIS-assisted large-scale wireless networks using stochastic geometry," *IEEE Trans. Wireless Commun.*, vol. 22, no. 11, pp. 7438–7451, Nov. 2023.

[28] Z. Ding, P. Fan, and H. V. Poor, "Impact of user pairing on 5G nonorthogonal multiple-access downlink transmissions," *IEEE Trans. Veh. Technol.*, vol. 65, no. 8, pp. 6010–6023, Aug. 2016.

[29] Z. Ding, Y. Liu, J. Choi, Q. Sun, M. Elkashlan, I. Chih-Lin, and H. V. Poor, "Application of non-orthogonal multiple access in LTE and 5G networks," *IEEE Commun. Mag.*, vol. 55, no. 2, pp. 185–191, Feb. 2017.

[30] D. Moltchanov, "Distance distributions in random networks," *Ad Hoc Networks*, vol. 10, no. 6, pp. 1146–1166, 2012. [Online]. Available: https://www.sciencedirect.com/science/article/pii/S1570870512000224

[31] J. G. Andrews, F. Baccelli, and R. K. Ganti, "A tractable approach to coverage and rate in cellular networks," *IEEE Trans. Commun.*, vol. 59, no. 11, pp. 3122–3134, Dec. 2011.

[32] W. Yi, Y. Liu, E. Bodanese, A. Nallanathan, and G. K. Karagiannidis, "A unified spatial framework for UAV-aided mmwave networks," *IEEE Trans. Commun.*, vol. 67, no. 12, pp. 8801–8817, Dec. 2019.

[33] Z. Ding, R. Schober, and H. V. Poor, "Unveiling the importance of sic in noma systemslpart 1: State of the art and recent findings," *IEEE Commun. Lett.*, vol. 24, no. 11, pp. 2373–2377, Nov. 2020.

[34] Y. Liu, X. Liu, X. Mu, T. Hou, J. Xu, M. Di Renzo, and N. Al-Dhahir, "Reconfigurable intelligent surfaces: Principles and opportunities," *IEEE Communications Surveys Tutorials*, vol. 23, no. 3, pp. 1546–1577, 2021.

[35] T. Bai and R. W. Heath, "Coverage and rate analysis for millimeter-wave cellular networks," *IEEE Trans. Wireless Commun.*, vol. 14, no. 2, pp. 1100–1114, Feb. 2015.

[36] C. Von Lanzenauer and W. Lundberg, "The n-fold convolution of a mixed density and mass function," *ASTIN Bulletin: The Journal of theIAA*, vol. 8, no. 1, pp. 99–103, 1974.

[37] C. Zhang, W. Yi, Y. Liu, Z. Ding, and L. Song, "STAR-IOS aided NOMA networks: Channel model approximation and performance analysis," *IEEE Trans. Wireless Commun.*, vol. 21, no. 9, pp. 6861–6876, Sep. 2022.

[38] A. Al-Hourani, S. Kandeepan, and S. Lardner, "Optimal lap altitude for maximum coverage," *IEEE Wireless Commun. Lett.*, vol. 3, no. 6, pp. 569–572, 2014.

[39] S. Atapattu, R. Fan, P. Dharmawansa, G. Wang, J. Evans, and T. A. Tsiftsis, "Reconfigurable intelligent surface assisted twocway communications: Performance analysis and optimization," *IEEE Trans Communications*, vol. 68, no. 10, pp. 6552–6567, Oct. 2020.

[40] T. Wang, M.-A. Badiu, G. Chen, and J. P. Coon, "Outage probability analysis of STAR-RIS assisted NOMA network with correlated channels," *IEEE Commun. Lett.*, vol. 26, no. 8, pp. 1774–1778, Aug 2022.

[41] B. Tahir, S. Schwarz, and M. Rupp, "Analysis of uplink IRS-assisted NOMA under nakagami-m fading via moments matching," *IEEE Wireless Commun. Lett.*, vol. 10, no. 3, pp. 624–628, Mar. 2021.

[42] X. Yu, Q. Cui, and M. Haenggi, "Coherent joint transmission in downlink heterogeneous cellular networks," *IEEE Wireless Commun. Lett.*, vol. 7, no. 2, pp. 274–277, Apr. 2018.

[43] H. Alzer, "On some inequalities for the incomplete Gamma function," *Math. Comput.*, vol. 66, no. 218, pp. 771–778, Apr. 1997.

[44] A. P. Prudnikov, Y. A. Brychkov, and O. I. Marichev, "*Integrals and series, vol. 1, special functions*," 1986.

[45] S. K. Gupta, V. Malik, A. K. Gupta, and J. G. Andrews, "Impact of blocking correlation on the performance of mmwave cellular networks," *IEEE Trans. Commun.*, vol. 70, no. 7, pp. 4925–4939, Jul. 2022.